UNIVERSITÀ DEGLI STUDI DI PADOVA

Dipartimento di Biologia

Corso di Laurea in Biologia Molecolare

Elaborato di laurea

Efficacia terapeutica della somministrazione di PKP2 mediata da virus adeno-associati nella cardiomiopatia aritmogena

Tutor: Prof.ssa Alessandra Rampazzo

Dipartimento di Biologia

Laureanda: Sara Cargnelutti

Anno accademico 2023/2024

Abstract

La cardiomiopatia aritmogena è una rara malattia ereditaria caratterizzata da gravi aritmie ventricolari, insufficienza cardiaca e morte improvvisa. Attualmente non esistono cure efficaci che ne arrestino lo sviluppo. Il 50% dei pazienti affetti da ACM possiede mutazioni nei geni che codificano proteine desmosomiali, tra cui la placofilina 2 (PKP2). Le mutazioni principali di questo gene determinano la produzione di trascritti che vengono spesso degradati portando a una condizione di aploinsufficienza che rappresenta una causa frequente di ACM. Nel lavoro analizzato in questo elaborato di laurea viene mostrato il potenziale curativo della somministrazione del gene PKP2 wild type utilizzando virus adeno-associati come vettori. Le analisi sono state condotte su tre modelli distinti: cardiomiociti derivati da cellule staminali pluripotenti indotte, miocardio umano ingegnerizzato e modello murino. I risultati ottenuti sono stati molto positivi e hanno permesso di andare oltre la fase pre-clinica.

Indice

In appendice viene allegato l'articolo scientifico discusso in questo elaborato di laurea

1. Introduzione

La cardiomiopatia aritmogena (ACM) è una rara malattia ereditaria caratterizzata da progressivi cambiamenti del miocardio che portano a gravi aritmie ventricolari (alterazioni del battito cardiaco), insufficienza cardiaca e morte improvvisa. L'incidenza di questa malattia varia da 1:2000 a 1:5000.

La diagnosi precoce è spesso impedita dalla complessità del fenotipo e dalla penetranza variabile. A stadi più avanzati, il rimodellamento del muscolo cardiaco diventa evidente con una sostituzione del miocardio con tessuto adiposo e fibroso, fino al raggiungimento dei risvolti clinici più gravi di questa patologia.

Il 50% dei pazienti affetti da ACM possiede mutazioni nei geni che codificano proteine desmosomiali: placofilina 2 (PKP2), placoglobina (JUP), desmoplachina (DSP), desmocollina (DSC2) e desmogleina (DSG2).

I desmosomi sono giunzioni di ancoraggio particolarmente resistenti alla trazione. Nel cuore, insieme alle giunzioni aderenti e comunicanti, costituiscono i dischi intercalari (ID), le strutture giunzionali che uniscono i cardiomiociti (Figura 1). Oltre a tenere unite le cellule tra loro, i dischi intercalari trasmettono la forza di trazione generata durante la contrazione e permettono la comunicazione elettrica necessaria per la trasmissione dell'impulso elettrico (accoppiamento elettrico-meccanico).

I desmosomi sono costituiti da due caderine desmosomiali (DSG2 e DSC2) e tre proteine di placca (DSP, JUP e PKP2). Le caderine sono molecole di adesione che interagiscono tra loro nello spazio intercellulare e sono collegate al citoscheletro per mezzo delle proteine adattatrici JUP, PKP2 e DSP. PKP2 interagisce con il suo dominio N-terminale con DSC2, DSP, JUP e con l'actina e i filamenti intermedi (desmina e cheratina) (Figura 1) [1].

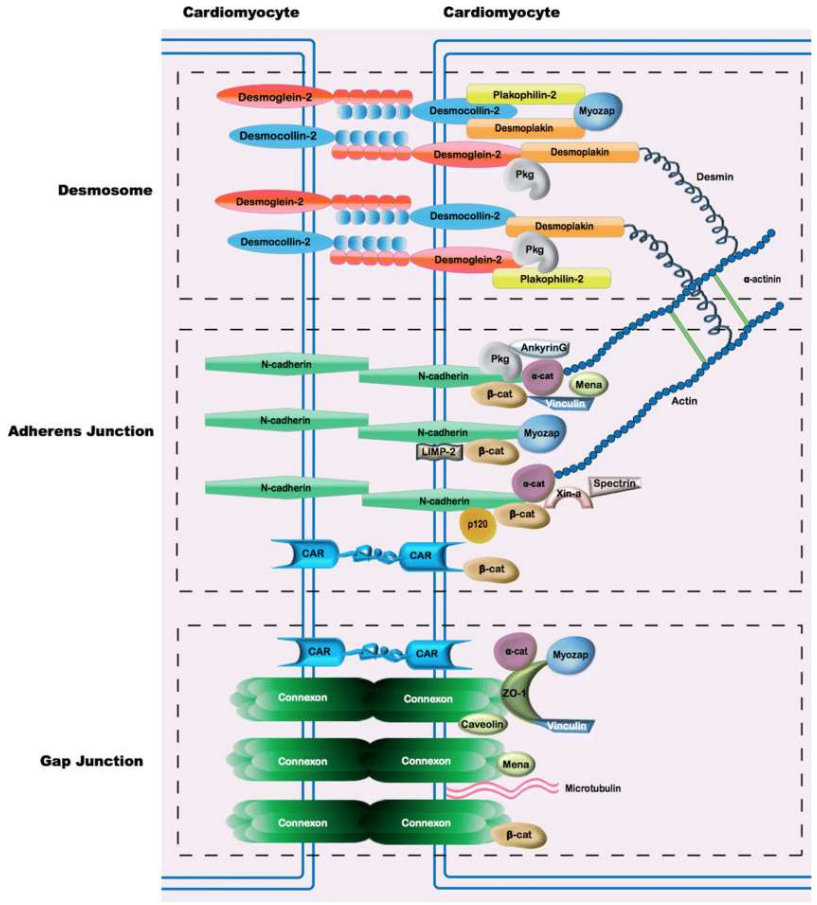

Figura 1 - Rappresentazione schematica dei desmosomi e delle altre strutture giunzionali (giunzioni aderenti e comunicanti) tra due cardiomiociti adiacenti. Si noti la localizzazione e le interazioni delle proteine desmosomiali coinvolte nell'ACM (da [1]).

PKP2 è il gene coinvolto principale, nello specifico PKP2 è associato all'insorgenza della cardiomiopatia aritmogena del ventricolo destro (ARVC), un sottotipo della malattia che colpisce maggiormente il ventricolo destro ed è principalmente ereditata con un pattern autosomico dominante.

Il gene PKP2 è localizzato sul braccio corto del cromosoma 12 ed è costituito da 15 esoni; sono note 10 varianti di splicing (fonte: NCBI).

Le mutazioni principali di questo gene determinano la produzione di trascritti tronchi che vengono spesso degradati per mezzo del nonsense mediated mRNA decay[1]. Ciò porta a una condizione di aploinsufficienza, in cui la quantità di proteina espressa solo dall'allele wild type non è sufficiente a garantire la corretta funzionalità del miocardio. L'aploinsufficienza di PKP2 è una causa frequente di ACM. I ruoli del gene PKP2 mutato nella genesi e nella progressione della malattia sono

molteplici. Interessante è la relazione diretta tra i livelli di PKP2 e quelli di altre proteine desmosomiali e di proteine delle giunzioni aderenti. Una ridotta quantità di PKP2 porta a instabilità desmosomiale ed eventuale degradazione delle proteine dell'area composita[2].

Sollecitazioni del miocardio con strutture giunzionali compromesse determinano il distacco e la morte dei cardiomiociti e la loro sostituzione con tessuto adiposo e fibroso. I principali meccanismi di morte dei cardiomiociti in ARVC sono: morte cellulare immunogenica, apoptosi, necroptosi e piroptosi [2]. Potrebbero anche verificarsi eventi di transdifferenziamento dei cardiomiociti in adipociti o fibrociti [3].

Non ci sono cure mirate ed efficaci per questa malattia, le attuali opzioni terapeutiche si basano sul trattamento della sintomatologia. In questo lavoro viene mostrato il potenziale curativo di una terapia genica basata sulla somministrazione esogena del gene PKP2 che agisce direttamente sulla causa.

Lo studio è stato condotto su una particolare mutazione del gene: $PKP2^{c.2013delC/WT}$, ovvero una mutazione in eterozigosi in cui in posizione 2013 del cDNA c'è la delezione di una citosina che causa un frameshift con conseguente codone di stop prematuro. Il ripristino di livelli adeguati della proteina PKP2 è stato ottenuto per mezzo della somministrazione del gene wild type mediata dal virus adeno-associato (AAV) con conseguente riformazione del complesso desmosomiale e miglioramento delle capacità contrattili.

Le analisi sono state condotte su tre modelli distinti: cardiomiociti derivati da cellule staminali pluripotenti indotte, miocardio umano ingegnerizzato (EHM) e topo.

---

1 Il nonsense mediated mRNA dacay è un sistema di controllo della qualità dei trascritti che permette di eliminare mRNA non full-length. Si basa sulla permanenza prolungata dell'exon junction complex (ECJ) sul trascritto a causa del distacco precoce del ribosoma per la presenza di un codone di stop prematuro. ECJ funziona così da marker di instabilità reclutando proteine che rimuovono il CAP inducendo una rapida degradazione del trascritto.

2 L'interazione tra le varie strutture giunzionali e la condivisione di alcuni elementi hanno portato a definire tutte le componenti dei ID come area composita.

2. Approccio sperimentale (materiali e metodi)

2.1 Cardiomiociti derivati da cellule staminali pluripotenti indotte

In questo studio sono state utilizzate delle cellule staminali pluripotenti indotte umane (hiPS), ovvero delle cellule pluripotenti ottenute mediante riprogrammazione cellulare a partire da cellule somatiche umane adulte, sulla base della tecnica messa appunto per la prima volta da Yamanaka e Takahashi nel 2006 in cellule di topo [4]. Nello specifico sono state utilizzate due linee cellulari iPS: una portatrice la mutazione PKP2 c.2013delC e una la mutazione PKP2 c.1854C>T.

Le cellule sono state fatte crescere ed espandere in adesione su pozzetti rivesti da Geltrex LDEV-Free, che è una forma solubile della membrana basale estratta da sarcoma murino. Come mezzo di coltura è stato usato Essential 8 (Gibco, A1517001) che è in grado di mantenere la pluripotenza delle cellule iPS. Quando in seguito a divisione, veniva raggiunto l'80-100% di confluenza, si effettuava il passaggio delle cellule (ovvero l'aspirazione del mezzo, la dissociazione delle cellule con un reagente apposito e la risemina in nuovi pozzetti). Al mezzo di coltura è stata aggiunta tiazovivina, un inibitore della chinasi associata a Rho (ROCK), che promuove la sopravvivenza delle cellule in seguito a separazione stabilizzando le E-caderine sulla superficie cellulare.

E' stato poi adottato un protocollo per indurre il differenziamento delle cellule pluripotenti in cardiomiociti. In questo modo si ottengono cellule del muscolo cardiaco che presentano il genoma del paziente a partire da fibroblasti o altre cellule somatiche riprogrammate. Il processo di differenziamento dei cardiomiociti a partire da cellule hiPS dura circa 30 giorni e inizia con l'induzione del mesoderma cardiaco [5]. I primi step di differenziamento sono realizzati in un medium low insulin, BSA-based con Polyvinyl Alcohol e Essential Lipids (LI-BPEL medium). Per indurre il differenziamento a mesoderma cardiaco, vengono aggiunti per 72h i seguenti componenti: Activina A, BMP4 e CHIR99021. Activina A e BMP4 sono due citochine appartenenti alla famiglia del TGF-beta, che ha diversi ruoli tra cui il controllo della proliferazione e del differenziamento cellulare. CHIR99021 è un attivatore della via di segnalazione Wnt[3]. Si può eventualmente usare un altro medium in cui mancano la maggior parte degli elementi presenti in LI-BPEL ma che include vari elementi presenti in

tracce (mBEL medium). Utilizzando questo medium, nel primo step non vengono usate le citochine, ma solo CHIR99021 per 48h.
A partire dal mesoderma cardiaco indotto da citochine si possono ottenere cardiomiociti aggiungendo XAV 939 e IWP-L6 per 48h (entrambi inibitori della via di segnalazione Wnt).

Per verificare la purezza, cioè quanti cardiomiociti sono stati ottenuti sul numero totale di cellule, è stata eseguita un'immunofluorescenza indiretta utilizzando anticorpi primari contro la troponina cardiaca T, una proteina specifica dei cardiomiociti. L'analisi è stata effettuata su $1x10^6$ cellule a 15 giorni d'età. Dopo aver ottenuto e lavato il pellet cellulare con Dulbecco's Phosphate-Bufferd Saline (dPBS), le cellule sono state fissate in etanolo freddo al 70%. Dopo di che è stata effettuata la permeabilizzazione delle membrane usando come detergente Triton X-100. Questo step è necessario al fine di permettere l'ingresso degli anticorpi nelle cellule. Queste sono state poi incubate con l'anticorpo primario in un buffer di blocking. Il buffer di blocking permette di bloccare siti di legame proteici aspecifici in modo che gli anticorpi leghino solo le proteine target. Dopo alcuni lavaggi per eliminare gli anticorpi che non si sono legati, è stata effettuata un'ulteriore incubazione in buffer di blocking con l'anticorpo secondario anti-coniglio Alexa 488. Alexa 488 è un dye fluorescente di colore verde a cui è coniugato l'anticorpo. Anche in questo caso sono stati effettuati i lavaggi per eliminare gli anticorpi che non si sono legati, prima di risospendere le cellule in dPBS per analizzarle con fluorescence-activated cell sorting (FACS), che permette di separare i cardiomiociti dalle altre cellule sulla base del segnale fluorescente emesso.

2.2 Patch clamp automatizzato

La tecnica del patch clamp si basa sull'utilizzo di una micro-pipetta di vetro per la formazione di un sigillo con la membrana plasmatica per effettuare misurazioni di corrente (bloccando il potenziale) e di potenziale (bloccando la corrente) sia a singolo canale sia in configurazione whole-cell, considerando dunque tutta la cellula.

3 La via di segnalazione Wnt è uno dei pathway principali nel differenziamento e nella proliferazione cellulare durante lo sviluppo. È attivata da proteine Wnt che si legano a recettori di membrana e agiscono da morfogeni, cioè stabiliscono un gradiente di concentrazione dalla sede di secrezione a quella di degradazione e le cellule assumono destini diversi sulla base della concentrazione di morfogeno a cui sono esposte.

In seguito a lavaggi con PBS e Versene e dissociazione con TrypLE Express, i cardiomiociti derivati da cellule iPS sono stati risospesi in HBSS divalent-free a 4°C. Per eseguire il patch clamp automatizzato è stato utilizzato lo strumento SyncroPatch 384 (Nanion Technologies). In configurazione whole-cell è stata registrata la corrente di sodio a 0,5 Hz per diversi valori di potenziale. Nel primo step l'holding potential è pari a -80mV, seguito da uno step iperpolarizzante di 100ms in cui si raggiungono -110mV e un test pulse di 300ms in cui il potenziale viene portato a -20mV. Le correnti registrate sono poi state analizzate con il software DataControl 384 (Nanion Technologies).

2.3 Generazione del miocardio umano ingegnerizzato

Uno dei limiti dei cardiomiociti ottenuti a partire da cellule hiPS è il loro basso livello di maturazione. A tale proposito si possono usare modelli 3D, come il miocardio umano ingegnerizzato (EHM), dove i cardiomiociti raggiungono livelli di maturazione maggiori, ottenendo così un modello con caratteristiche strutturali e funzionali del miocardio post-natale che si presta ad analisi di PKP2, avendo questa proteina un ruolo chiave nell'interazione e nel legame tra le cellule.

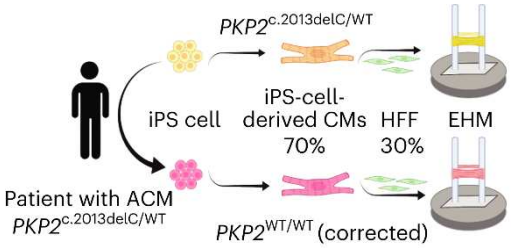

Figura 2 – Rappresentazione schematica del processo di ottenimento di EHM a partire da cardiomiociti ottenuti da cellule hiPS.

Il protocollo è stato eseguito sia a partire dalla linea cellulare mutata che da quella wild type (Figura 2). Per ottenere EHM, i cardiomiociti ottenuti da cellule hiPS sono stati uniti a fibroblasti di origine umana (HFF-1, ATCC, SCRC-1041) in rapporto 70:30 [6]. Il ruolo dei fibroblasti è quello di "feeder cells", cioè quello di secernere componenti di matrice extra-cellulare e fattori di crescita. Il mix di cellule è stato risospeso in collagene di tipo 1 diluito nel medium RPMI 1640 e poi versato in una piastra multi-pozzetto per EHM, nello specifico la myrPlate-TM5 (myriamed GmbH). In ogni pozzetto sono presenti due miniaste flessibili (Figura 2) che supportano la crescita del tessuto in una forma ad anello con un carico meccanico definito. Dopo 45 minuti di incubazione a 37°, viene aggiunto nuovo medium con TGF-beta1. Questa aggiunta viene ripetuta per i successivi tre giorni.

2.4 Analisi della contrazione

In EHM, la contrazione è stata misurata con registrazioni video-ottiche della curvatura mediata da EHM delle aste presenti nei pozzetti della piastra myrPlate-TM5 a 37°. Le contrazioni spontanee sono state registrate per almeno due minuti a 50 fotogrammi per secondo. La percentuale di curvatura delle aste viene considerata come una misura che rappresenta la forza di contrazione (F). Le velocità di contrazione e di rilassamento corrispondono al massimo e al minimo, rispettivamente, di dF/dt.

2.5 Western blot

Il western blot, o immuno blot, è una procedura di blotting in cui vengono utilizzati anticorpi per individuare le proteine target. Questa tecnica è stata applicata su estratto proteico ottenuto dai cardiomiociti derivati da cellule iPS. Sono stati utilizzati anticorpi primari che si legano proteine desmosomiali e anticorpi secondari coniugati alla perossidasi di rafano che catalizza una reazione che rilascia luce. L'immuno blot è stato eseguito anche per l'analisi della composizione dei desmosomi in EHM e in estratti proteici ottenuti da tessuto ventricolare di topo congelato.

2.6 Quantitative real-time PCR

Dai cardiomiociti derivati da cellule iPS è stato estratto l'RNA, da cui poi è stato sintetizzato il DNA complementare, substrato della PCR quantitativa utilizzata per valutare il livello di espressione di vari geni. La PCR è stata realizzata con CFX96 Realtime PCR system e iQ SYBR Green supermix (entrambi Bio-Rad), contenente come dye il SYBR Green I e come enzima l'hot-start iTaq DNA polimerasi. La real-time PCR è stata eseguita anche per mRNA estratto da EHM per valutare i livelli di espressione di ACTN2, VIM, DCN e NPPB. I dati sono stati normalizzati usando GUS come gene housekeeping.

2.7 Modello murino

Per le analisi in vivo è stato utilizzato il modello murino $Pkp2^{c.1755delA/WT}$. Gli studi su cuccioli di topo sono stati condotti sia su individui maschi che individui femmine, mentre quelli su topi adulti sono stati condotti solo su individui di genere maschile.

2.8 Ecocardiografia

Le analisi ecocardiografiche fanno riferimento a varie tecniche poco invasive che si basano sull'utilizzo di ultrasuoni per creare immagini del cuore. È stato usato un dispositivo visivo a ultrasuoni collegato a un trasduttore di 30MHz per eseguire le misurazioni di diversi parametri cardiaci, come la velocità di riempimento ventricolare precoce (E) e tardivo (A) (da cui si calcola il rapporto E/A) e IVRT[4]. A partire da questi parametri, si può calcolare automaticamente la funzione cardiaca con un software, in particolare la frazione di eiezione che rappresenta la capacità del ventricolo di contrarsi e far fuoriuscire il sangue.

2.9 Immunofluorescenza e immunoistochimica

Per tessuto cardiaco murino è stata eseguita un'analisi di immunoistochimica e per EHM un'analisi di immunofluorescenza. Entrambe le tecniche si basano sull'utilizzo di anticorpi per la visualizzazione delle proteine a cui si legano, ciò che cambia è il metodo di rilevazione: l'immunofluorescenza si basa sulla presenza di dye fluorescenti legati all'anticorpo secondario, mentre l'immunoistochimica su enzimi come la perossidasi o la fosfatasi. I campioni sono stati fissati in paraformaldeide, inclusi in paraffina e poi sezionati. Le sezioni di tessuto (spessore: 4μm) sono state poi decerate e reidratate. Successivamente sono state bollite per 20 minuti in EDTA o sodio citrato e poi bloccate per 45 minuti a temperatura ambiente usando una soluzione contenente albumina sierica bovina e TWEEN20 disciolto in dPBS. Dopo l'incubazione con anticorpi primari e secondari, è stata effettuata la colorazione con DAPI (dye fluorescente per la visualizzazione del DNA) e montaggio su vetrino con Mowiol per la visualizzazione al microscopio.

2.10 Virus adeno-associati

I virus adeno-associati sono particelle virali con capside icosaedrico, prive di envelope, il cui genoma è costituito da una molecola di DNA a singolo filamento di circa 4,8 kb che contiene tre geni: Rep (Replication), Cap (Capsid) e aap (Assembly) [7]. I geni sono fiancheggianti da due sequenze terminali ripetute (ITRs) necessarie alla replicazione e al packaging.

4 IVRT è il tempo di rilassamento isovolumico e corrisponde all'intervallo del ciclo cardiaco che intercorre tra la chiusura della valvola aortica e l'apertura della valvola mitrale. È un indicatore di disfunzione diastolica.

Questi virus possono essere ingegnerizzati per veicolare DNA di interesse in cellule target. Al posto dei geni virali, tra le due ITRs viene inserita una cassetta di espressione con i geni e i promotori desiderati. In questo studio, gli AAV sono stati utilizzati come vettori del gene codificante la proteina PKP2, oppure come vettori vuoti di controllo. Il sierotipo 6 è stato utilizzato per infettare cardiomiociti derivati da iPS (sia di coltura 2D sia di EHM) e il sierotipo 9 per infettare i topi (Figura 3).

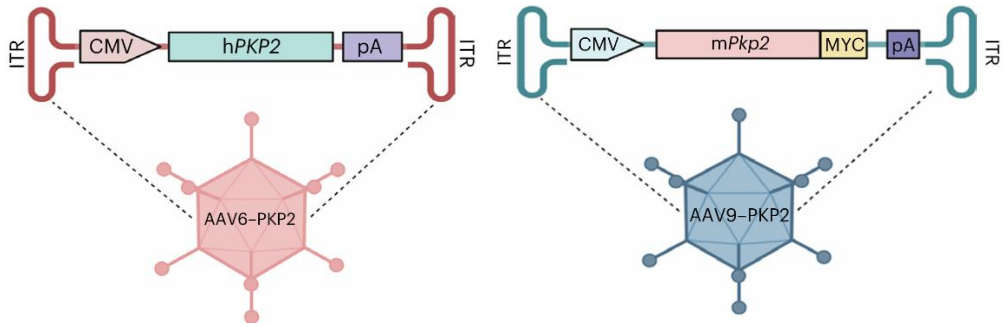

Figura 3 – Rappresentazione schematica dei vettori AAV6 (sinistra) e AVV9 (destra) e delle relative cassette di espressione utilizzate.

In entrambe le cassette è stato utilizzato un promotore immediate-early di citomegalovirus (CMV). Il gene Pkp2 in AAV9 è fuso con il gene codificante l'epitopo MYC che permette di rilevare la proteina PKP2 di origine esogena, distinguendola da quella endogena, in un saggio di immunoistochimica. pA è il sito di poliadenilazione.

2.11 Analisi statistiche

È stato eseguito il test t di Student per determinare se la differenza tra i dati ottenuti relativi a due gruppi (dipendenti o indipendenti) è statisticamente significativa o meno. In caso di un numero di gruppi maggiore a due, è stato eseguito un test post-hoc appropriato per l'analisi della varianza (ANOVA). I test statistici sono stati effettuati con il software GraphPad Prism 9.5.1.

3. Risultati

3.1 Risultati ottenuti in cardiomiociti ottenuti da cellule iPS

È stata effettuata la trasduzione del vettore AAV6 che esprime il gene PKP2 wild type (AAV6-PKP2) nella linea cellulare mutata e sono state generate cellule isogeniche come controllo, ovvero cellule in cui la mutazione è stata corretta per ottenere un genotipo wild type. L'esperimento è stato ripetuto per due cariche virali diverse ($0{,}5x10^3$ e $5x10^3$ genomi virali per cellula) al fine di individuare il dosaggio adatto. È emerso che i livelli di PKP2 dipendono dalla carica virale e con la carica più alta si ha il completo ripristino del livello di PKP2 nei cardiomiociti mutati. Per capire quali sono gli effetti di questo recupero sulla struttura dei desmosomi, alcuni cardiomiociti mutati sono stati trasdotti con il vettore AAV6-PKP2, altri con un vettore vuoto di controllo (AAV6-ctr). Come reference, sono stati trasdotti cardiomiociti privi della mutazione con AAV6-ctr. Dopo 4 giorni è stato isolato l'RNA e dopo 7 giorni le proteine. La real-time PCR non ha mostrato effetti rilevanti sui livelli di mRNA delle altre proteine desmosomiali (JUP, DSP, DSG2, DSC2) né in cellule mutate infettate con AAV6-ctr, né in cellule mutate infettate con AAV6-PKP2 rispetto al reference. Il western-blot, invece, mostra che il ripristino dei livelli di PKP2 porta al recupero anche delle proteine JUP e DSP (i cui livelli erano diminuiti insieme a quello di PKP2 in cellule mutate infettate con AAV6-ctr), mentre i livelli delle proteine DSC2 e DSG2 rimangono inalterati (la quantità di DSC2 non diminuisce in conseguenza alla mutazione di PKP2; DSG2 diminuisce, ma poi non aumenta in seguito alla trasduzione). Gli stessi esperimenti sono stati condotti anche su cardiomiociti che presentano un'altra mutazione in PKP2 ($PKP2^{c.1854C>T/WT}$) e hanno avuto esiti analoghi. Questi risultati indicano dunque che il recupero di livelli fisiologici della proteina PKP2 migliora i livelli delle proteine desmosomiali e quindi l'assemblaggio dei desmosomi nei cardiomiociti con mutazioni nel gene PKP2 che determinano aploinsufficienza.

Diversi studi riportano che una delle conseguenze dell'aploinsufficienza di PKP2 è una corrente del sodio (I_{Na}) alterata, che è legata a gravi aritmie ventricolari. È stato dunque eseguito un esperimento di patch clamp automatizzato high-throughput per analizzare I_{Na} in cardiomiociti con la mutazione e in cardiomiociti isogenici di controllo. È stata registrata una notevole riduzione di I_{NA} in cellule mutanti, dimostrando che questo

modello replica il substrato aritmico caratteristico di ACM. È stata poi valutata l'efficacia terapeutica della somministrazione esogena del gene di PKP2 mediata da AAV6. I dati rivelano che la conduzione del sodio in cellule della linea mutata è riportata a livelli comparabili a quelli della linea cellulare wild type.

3.2 Risultati ottenuti in EHM

É stata valutata l'espressione genica di markers cardiaci (come α-actinina-2 (ACTN2)) e fibroblastici (come vimentina (VIM) e decorina (DCN)) in EHM ottenuto da cardiomiociti mutati (EHM $PKP2^{c.2013delC/WT}$) e wild type (EHM $PKP2^{WT/WT}$). In EHM $PKP2^{c.2013delC/WT}$, l'espressione di ACTN2 diminuisce, mentre aumenta quella di VIM e DCN rispetto al controllo isogenico. In EHM $PKP2^{c.2013delC/WT}$ c'è anche una maggiore espressione del gene NPPB, che codifica una proteina facente parte della famiglia dei peptidi natriuretici che viene secreta e funziona da ormone cardiaco; un'elevata concentrazione di questa proteina nel circolo sanguigno è indicativa di insufficienza cardiaca.

Con l'osservazione dei tessuti utilizzando il tricromo di Masson[5], non sono state rinvenute importanti differenze relative alla fibrosi (deposizione di tessuto connettivo fibroso in seguito a danno), nonostante le differenze trascrizionali sovracitate.

È stato poi effettuato un saggio di immunofluorescenza in EHM di sei settimane valutando la localizzazione delle proteine N-caderina (NCAD) e PKP2. Nel tessuto di controllo, rispetto a quello mutato, è visibile una struttura più simile a quella dei dischi intercalari. In entrambi i casi, l'organizzazione delle giunzioni è migliore rispetto al modello 2D.

La composizione dei desmosomi è stata analizzata mediante western blot. I risultati indicano una diminuzione nel tessuto mutato delle proteine PKP2, JUP e DSP e delle caderine DSC2 e DSG2. Da notare il calo di DSC2 che non era stato osservato nel modello 2D, ciò può essere dovuto a una minore maturazione dei cardiomiociti nel modello bidimensionale o allo stress meccanico presente in EHM.

5 Il tricromo di Masson è una tecnica di colorazione istologica a tre colori, particolarmente adatta all'osservazione del tessuto connettivo in quanto mette in evidenza le fibre di collagene (colore blu).

Registrazioni video-ottiche della contrazione di EHM hanno dimostrato una diminuzione significativa della forza di contrazione in EHM mutato.

Sono stati infine generati EHM a partire da cardiomiociti ottenuti da cellule iPS (sia mutati che wild type) preventivamente infettati con AAV6-PKP2 o AAV6-ctr. In EHM $PKP2^{c.2013delC/WT}$ infettato con AAV6-PKP2, si è osservato un aumento dei livelli di PKP2 6 settimane dopo la formulazione di EHM, oltre che a quelli di JUP, DSP e DSG2 (non DSC2) e a quelli di altre proteine di ID, come NCAD e αCAT. Quest'ultima evidenza sperimentale potrebbe implicare la formazione di giunzioni più forti. L'over-espressione di PKP2 in EHM $PKP2^{WT/WT}$ infettato con AAV6-PKP2 non porta a un aumento significativo della quantità di PKP2, né delle altre proteine di ID prese in considerazione.

Da un punto di vista funzionale, la trasduzione di AAV6-PKP2 ha portato a un progressivo miglioramento dell'ampiezza di contrazione e a una normalizzazione delle cinetiche di contrazione alterate. È stata osservata l'assenza di effetti collaterali nelle proprietà contrattili di EHM wild type infettato con AAV6-PKP2.

In conclusione, possiamo dire che questi risultati dimostrano un miglioramento sia dal punto di vista molecolare che funzionale in EHM $PKP2^{c.2013delC/WT}$ in seguito alla somministrazione del gene di PKP2 AAV6-mediata.

3.3 Risultati ottenuti nel modello murino

In topo è stata presa in considerazione la mutazione $Pkp2^{c.1755delA/WT}$, che è l'equivalente murino della mutazione $PKP2^{c.2013delC/WT}$ in uomo. In topi con genotipo mutato si osserva una diminuzione dei livelli di PKP2 e anche di altre proteine desmosomiali e proteine delle giunzioni aderenti. Per la somministrazione esogena di Pkp2 è stato utilizzato AAV9 come vettore (AAV9-PKP2). Inizialmente il vettore ($2x10^{14}$ genomi virali/Kg) è stato somministrato per via intraperitoneale in topi sia mutati che wild type a 5 giorni d'età. I tessuti sono stati estratti e analizzati 2 settimane dopo l'iniezione. L'efficienza di trasduzione è risultata essere pari a circa il 76%, quindi in 3 cardiomiociti su 4 circa è avvenuta la trasduzione di AAV9. È stato fatto un saggio di immunoistochimica per valutare la posizione di PKP2 di origine esogena su sezioni di tessuto cardiaco incluso in paraffina da cui si conclude che la proteina si colloca correttamente all'interno di ID. L'immunoblot in topi mutati infettati con AAV9-PKP2 conferma il recupero dei livelli di PKP2, oltre a quelli della proteina JUP e un parziale recupero

di DSP e DSG2; i livelli di DSC2 risultano essere indipendenti rispetto a quelli di PKP2. Questi risultati sono in accordo con quelli ottenuti in EHM.

È stata poi effettuata l'iniezione endovena di AAV9-PKP2 o AAV9-ctr in topi Pkp2 mutanti e wild type di due mesi, in quanto i sintomi di ACM spesso si manifestano in giovane età adulta. È stato utilizzato un dosaggio di $5x10^{13}$ genomi virali/Kg ed ottenuta un'efficienza di trasduzione del 71% nel ventricolo sinistro. I tessuti sono stati isolati e analizzati due settimane dopo l'iniezione. Il recupero dei livelli di PKP2 è accompagnato anche da quello delle altre proteine desmosomiali (tranne DSC2, che si dimostra sempre indipendente rispetto a PKP2) e delle proteine delle giunzioni aderenti come NCAD e α-CAT, analogamente a quanto ottenuto in EHM.

Successivamente, è stata iniettata una singola dose di $3x10^{13}$ genomi virali/Kg di AAV9-ctr o AAV9-PKP2 in topi sia mutati che wild type di due mesi al fine di indagare le conseguenze della somministrazione di Pkp2 a 4, 8 e 12 mesi d'età. Si sono manifestate progressive disfunzionalità cardiache, come la diminuzione del rapporto E/A e un aumento di IVRT. Il saggio di immunoistochimica indica la localizzazione di PKP2 esogena in ID nel tessuto cardiaco di topi a 12 mesi d'età dopo una sola iniezione. Il western blot, eseguito su cellule ottenute da topi mutati di 12 mesi trattati con AAV9-PKP2, rivela un aumento di PKP2, JUP, DSP e DSG2; a differenza degli altri modelli con un livello di maturazione dei cardiomiociti inferiore, anche la proteina DSC2 risulta responsiva, diminuendo con la mutazione e aumentando inseguito a iniezione di AAV9-PKP2. In topi wild type infettati con AAV9-PKP2 non si osservano aumenti rilevanti di PKP2 nè delle altre proteine desmosomiali, in linea con quanto era stato osservato in EHM. Sono state eseguite anche analisi ecocardiografiche a vari mesi d'età e queste non hanno rilevato differenze significative relative a varie misure funzionali e morfologiche cardiache tra topi wild type e mutati. Tali misure non sono state influenzate nemmeno dalla somministrazione di AAV9-ctr o AAV9-PKP2, supportando così l'ipotesi che l'over-espressione di Pkp2 non determini un fenotipo cardiaco alterato. In topi mutati trattati di 12 mesi, si è osservato un miglioramento di E/A e IVRT.

Dall'analisi di altri organi (come polmone, fegato, milza e reni) che sono inclini a essere infettati da AAV9, è risultato un basso livello di espressione di PKP2 esogena nel fegato, che potrebbe essere dovuto all'elevato tropismo dei virus AAV per le cellule epatiche.

Nel complesso, questi risultati ottenuti in vivo mostrano miglioramenti sia da un punto di vista molecolare, sia per quanto riguarda la funzionalità cardiaca in seguito alla somministrazione di una singola dose di AAV9-PKP2 in topi che presentano la mutazione $Pkp2^{c.1755delA/WT}$ e non sono stati rilevati particolari effetti collaterali né a livello cardiaco, né in altri organi.

4. Conclusione e analisi critica

In questo studio è stato valutato il potenziale terapeutico del recupero dei livelli della proteina PKP2 mediato da virus adeno-associati per persone che presentano mutazioni nel gene PKP2 determinanti aploinsufficenza, condizione che rappresenta una delle cause più frequenti della cardiomiopatia aritmogena. Si tratta di uno studio pilota che utilizza la terapia genica basata sugli AAV, già utilizzata per diverse patologie, nell'ambito della cardiomiopatia aritmogena. Sono stati analizzati gli effetti in tre diversi modelli, ciascuno dei quali si presta ad analisi diverse. Nel complesso, le analisi hanno dimostrato miglioramenti a livello molecolare (aumentata espressione di PKP2 e altre proteine desmosomiali), strutturale (miglior assemblamento dei desmosomi) e funzionale (miglioramento della fisiologia cardiaca e.g. conduzione del sodio e capacità contrattili). Viene anche dimostrato come l'overespressione di PKP2 in cellule sane non abbia effetti negativi, potrebbe dunque essere presente un meccanismo cellulare che mantiene le proteine a livelli fisiologici degradandone l'eccesso. Questo è punto molto importante per l'applicazione della terapia genica, perché non si può prevedere con esattezza i livelli della proteina raggiunti nelle cellule in seguito a trasduzione, livelli superiori a quelli fisiologici potrebbero risultare dannosi.

Un aspetto che va considerato è il numero di cardiomiociti che vengono infettati in vivo. Efficacia di trasduzione pari a circa il 70% nei ventricoli di topo si è dimostrata essere sufficiente. Affinché il virus infetti i cardiomiociti e non altri off-targets bisogna utilizzare un promotore specifico per il cuore, un capside cardiotropico (come la chimera ottenuta dai sierotipi AAV2 e AAV8) ed eventualmente delle sequenze detarget specifiche (ad esempio contro le cellule epatiche, visto che sono stati rilevate PKP2 esogene in quest'organo). Un altro punto critico delle terapie geniche basate sugli AAV

è il possibile sviluppo di una risposta immunitaria sia innata che adattativa contro il vettore virale da parte dei pazienti, soprattutto quelli che sono già venuti in contatto con il virus e che hanno quindi sviluppato memoria immunologica [8].

Questo approccio terapeutico è applicabile in condizioni patologiche determinate da mutazioni che portano alla degradazione dei trascritti, non risulta dunque applicabile per mutazioni d'altro tipo (e.g missenso) in cui si producono trascritti alterati che non vengono degradati. Va sottolineato, inoltre, che questa terapia genica è gene-specifica e per trattare patologie determinate da mutazioni in altri geni, bisogna creare un nuovo vettore virale e ripetere le analisi.

Nell'ambito delle altre possibili terapie di tipo genico attualmente disponibili, quella basata sugli AAV, che prevede di veicolare all'interno delle cellule il gene wild type, si affianca alla strategia di gene editing CRISPR/Cas9, che prevede invece la correzione della mutazione [9]. Questa tecnologia rivoluzionaria mostra però ancora applicazioni limitate in ambito clinico, soprattutto per la possibilità di introdurre varianti nucleotidiche indesiderate e potenzialmente dannose.

Per individuare i pazienti che potrebbero beneficiare di questa terapia si possono utilizzare test genetici, anche se sono riservati a persone che presentano familiarità o con problemi cardiaci diagnosticati. I test genetici non sono comunque necessariamente informativi su quanto accade a livello proteico. Un metodo per determinare il livello delle proteine desmosomiali in maniera indiretta potrebbe basarsi sull'analisi di altre cellule informative; è stato dimostrato, ad esempio, che i livelli di PKP2 nei cheratinociti rispecchiano i livelli di PKP2 nei cardiomiociti.

I risultati di questo ed altri studi hanno portato all'avvio di trial clinici attualmente sponsorizzati da tre case farmaceutiche (Lexeo Therapeutics, Tenaya Therapeutics e Rocket Pharmaceuticals) (fonte: clinicaltrials.gov). Al momento i trial si trovano in fase 1 con il reclutamento di pazienti che rispettino i criteri di ammissibilità al fine di analizzare la tollerabilità, l'eventuale tossicità, l'espressione del gene veicolato e individuare i dosaggi adatti. I tre trial sono iniziati tra la fine del 2023 e l'inizio del 2024 e prevedono tempistiche diverse con la loro conclusione tra il 2026 e il 2029.

Bibliografia

[1] Zhao G, Qiu Y, Zhang HM, Yang D. Intercalated discs: cellular adhesion and signaling in heart health and diseases. Heart Fail Rev. 2019,24:115-132. doi: 10.1007/s10741-018-9743-7.

[2] Lu W, Rao Y, Li Y, Dai Y, Chen K. The Landscape of Cell Death Processes with Associated Immunogenic and Fibrogenic Effects in Arrhythmogenic Cardiomyopathy. J Cardiovasc Dev Dis. 2022 Sep 8;9(9):301. doi: 10.3390/jcdd9090301. PMID: 36135446; PMCID: PMC9500988.

[3] d'Amati G, di Gioia CR, Giordano C, Gallo P. Myocyte transdifferentiation: a possible pathogenetic mechanism for arrhythmogenic right ventricular cardiomyopathy. Arch Pathol Lab Med. 2000 Feb;124(2):287-90. doi: 10.5858/2000-124-0287-MT. PMID: 10656741.

[4] Takahashi K, Yamanaka S. Induction of pluripotent stem cells from mouse embryonic and adult fibroblast cultures by defined factors. Cell. 2006 Aug 25;126(4):663-76. doi: 10.1016/j.cell.2006.07.024. Epub 2006 Aug 10. PMID: 16904174.

[5] Campostrini G, Meraviglia V, Giacomelli E, van Helden RWJ, Yiangou L, Davis RP, Bellin M, Orlova VV, Mummery CL. Generation, functional analysis and applications of isogenic three-dimensional self-aggregating cardiac microtissues from human pluripotent stem cells. Nat Protoc. 2021 Apr;16(4):2213-2256. doi: 10.1038/s41596-021-00497-2. Epub 2021 Mar 26. PMID: 33772245; PMCID: PMC7611409.

[6] Tiburcy M, Hudson JE, Balfanz P, Schlick S, Meyer T, Chang Liao ML, Levent E, Raad F, Zeidler S, Wingender E, Riegler J, Wang M, Gold JD, Kehat I, Wettwer E, Ravens U, Dierickx P, van Laake LW, Goumans MJ, Khadjeh S, Toischer K, Hasenfuss G, Couture LA, Unger A, Linke WA, Araki T, Neel B, Keller G, Gepstein L, Wu JC, Zimmermann WH. Defined Engineered Human Myocardium With Advanced Maturation for Applications in Heart Failure Modeling and Repair. Circulation. 2017 May 9;135(19):1832-1847. doi: 10.1161/CIRCULATIONAHA.116.024145. Epub 2017 Feb 6. PMID: 28167635; PMCID: PMC5501412.

[7] Naso MF, Tomkowicz B, Perry WL 3rd, Strohl WR. Adeno-Associated Virus (AAV) as a Vector for Gene Therapy. BioDrugs. 2017 Aug;31(4):317-334. doi: 10.1007/s40259-017-0234-5. PMID: 28669112; PMCID: PMC5548848.

[8] Kolesnik VV, Nurtdinov RF, Oloruntimehin ES, Karabelsky AV, Malogolovkin AS. Optimization strategies and advances in the research and development of AAV-based gene therapy to deliver large transgenes. Clin Transl Med. 2024 Mar;14(3):e1607. doi: 10.1002/ctm2.1607. PMID: 38488469; PMCID: PMC10941601.

[9] Jiang F, Doudna JA. CRISPR-Cas9 Structures and Mechanisms. Annu Rev Biophys. 2017 May 22;46:505-529. doi: 10.1146/annurev-biophys-062215-010822. Epub 2017 Mar 30. PMID: 28375731.

nature cardiovascular research

Article

https://doi.org/10.1038/s44161-023-00378-9

Therapeutic efficacy of AAV-mediated restoration of PKP2 in arrhythmogenic cardiomyopathy

Received: 19 May 2023

Accepted: 27 October 2023

Published online: 7 December 2023

Check for updates

Eirini Kyriakopoulou[1], Danielle Versteeg[1], Hesther de Ruiter[1], Ilaria Perini[1], Fitzwilliam Seibertz[2,3,4,5], Yannic Döring[2,3], Lorena Zentilin[6], Hoyee Tsui[1], Sebastiaan J. van Kampen[1], Malte Tiburcy[2,3], Tim Meyer[2,3], Niels Voigt[2,3,4], van J. Peter Tintelen[7], Wolfram H. Zimmermann[2,3,4,8,9], Mauro Giacca[6,10] & Eva van Rooij[1,11]

Arrhythmogenic cardiomyopathy is a severe cardiac disorder characterized by lethal arrhythmias and sudden cardiac death, with currently no effective treatment. Plakophilin 2 (*PKP2*) is the most frequently affected gene. Here we show that adeno-associated virus (AAV)-mediated delivery of PKP2 in *PKP2*$^{c.2013delC/WT}$ induced pluripotent stem cell-derived cardiomyocytes restored not only cardiac PKP2 levels but also the levels of other junctional proteins, found to be decreased in response to the mutation. PKP2 restoration improved sodium conduction, indicating rescue of the arrhythmic substrate in *PKP2* mutant induced pluripotent stem cell-derived cardiomyocytes. Additionally, it enhanced contractile function and normalized contraction kinetics in *PKP2* mutant engineered human myocardium. Recovery of desmosomal integrity and cardiac function was corroborated in vivo, by treating heterozygous *Pkp2*$^{c.1755delA}$ knock-in mice. Long-term treatment with AAV9–PKP2 prevented cardiac dysfunction in 12-month-old *Pkp2*$^{c.1755delA/WT}$ mice, without affecting wild-type mice. These findings encourage clinical exploration of PKP2 gene therapy for patients with PKP2 haploinsufficiency.

Arrhythmogenic cardiomyopathy (ACM) is a progressive genetic cardiac disorder with a prevalence ranging from 1:2,000 to 1:5,000 (ref. 1). Early diagnosis is often hindered by phenotypic complexity and variable disease penetrance[2]. At the clinically concealed phase of the disease, patients often present asymptomatic or with mild electrocardiogram abnormalities, while possessing high risk of sudden cardiac death[3]. As disease progresses, structural remodeling characterized by fibro-fatty tissue infiltration within the myocardium becomes evident, ultimately leading to life-threatening ventricular arrhythmias and heart failure, a condition that often requires heart transplantation[3,4].

[1]Hubrecht Institute-KNAW and Utrecht University Medical Center, Utrecht, the Netherlands. [2]Institute of Pharmacology and Toxicology, University Medical Center Gottingen (UMG), Göttingen, Germany. [3]German Center for Cardiovascular Research (DZHK), partner site Göttingen, Göttingen, Germany. [4]Cluster of Excellence 'Multiscale Bioimaging: from Molecular Machines to Networks of Excitable Cells' (MBExC), University of Göttingen, Göttingen, Germany. [5]Nanion Technologies GmbH, Munich, Germany. [6]International Centre for Genetic Engineering and Biotechnology (ICGEB), Trieste, Italy. [7]Department of Genetics, University Medical Centre Utrecht, Utrecht, the Netherlands. [8]German Center for Neurodegenerative Diseases (DZNE), Göttingen, Germany. [9]Fraunhofer Institute for Translational Medicine and Pharmacology (ITMP), Göttingen, Germany. [10]British Heart Foundation Centre of Research Excellence, School of Cardiovascular Medicine & Sciences, King's College London, London, UK. [11]Department of Cardiology, University Medical Center Utrecht, Utrecht, the Netherlands. e-mail: e.vanrooij@hubrecht.eu

Approximately 50% of patients with ACM carry genetic mutations in the desmosomal genes: plakophilin 2 (*PKP2*), plakoglobin (*JUP*), desmoplakin (*DSP*), desmocollin (*DSC2*) and desmoglein (*DSG2*)[5]. Desmosomes are robust multiprotein structures localized within the intercalated discs (IDs), where they facilitate mechanical coupling of the adjacent cardiomyocytes (CMs)[6]. Despite the classical notion that desmosomes function individually, a close connection and interaction of desmosomes with more ID components such as ion channels, gap junctions and adherens junctions has been described, together forming the area composita or connexome[6–9].

PKP2 is the most commonly affected gene in patients with ACM[10]. Specifically, mutations in *PKP2* have been strongly associated with the onset and development of arrhythmogenic right ventricular cardiomyopathy, a distinctive subtype of ACM marked by its pronounced impact on the right ventricle. While there is growing evidence revealing contributions from both the biventricular and left ventricular regions to the ACM phenotype, it is worth noting that arrhythmogenic right ventricular cardiomyopathy continues to be the predominant subtype within the ACM spectrum, primarily inherited through an autosomal dominant pattern[11]. The vast majority of genetic alterations affecting *PKP2* are truncating variants[12]. These mutant transcripts are often degraded by nonsense-mediated messenger RNA decay, causing PKP2 haploinsufficiency, which is an important pathogenic ACM driver[12–14]. The fundamental role of PKP2 in ACM disease pathogenesis and progression has been highlighted by several studies[9,14–22]. A study on a cardiomyocyte-specific, inducible deletion of *Pkp2* in mice revealed PKP2 as a crucial regulator of calcium cycling and cardiac rhythm[15]. These findings were further corroborated on a heterozygous *Pkp2* knockout mouse model exposed to environmental stress stimuli[22]. Another study demonstrated endogenous correlation of *PKP2* transcript abundance with the abundance of transcripts encoding inflammatory/immune response factors, the presence of which is thought to mediate ACM progression[17]. Interestingly, a study aiming to explore the pathogenic mechanisms leading to ventricular dilation and decreased systolic function associated with ACM, revealed that truncating *PKP2* mutations impair CM contractility by disrupting sarcomere stability and localization[14]. Of relevance, it was recently shown that cardiac levels of PKP2 directly correlate to protein levels of other desmosomal and adherens junction proteins in patients[20]. These data suggest that PKP2 fulfills a key anchoring role for the stabilization and function of other desmosomal and ID proteins. PKP2 loss as a consequence of truncating variants induces desmosomal instability and the eventual degradation of the area composita-related proteins, whereby downstream disease processes become activated.

Despite an improvement in our knowledge about the molecular triggers underlying ACM, targeted and effective therapeutic interventions for this disease remain lacking. While current treatment options are more focused on treating disease symptoms[23], targeting the primary cause of disease consequently leading to ACM would have curative potential.

Here we show that adeno-associated virus (AAV)-mediated PKP2 restoration results in the re-formation of the desmosomal complex and consequently an improvement in contractile function in *PKP2*$^{c.2013delC/WT}$ induced pluripotent stem (iPS) cell-derived CMs, *PKP2*$^{c.2013delC/WT}$ engineered human myocardium (EHM) and *Pkp2* mutant knock-in mice. Molecular restoration of desmosomal and non-desmosomal protein components within the ID was observed following exogenous administration of *Pkp2*, which successfully prevented the functional decline induced by PKP2 haploinsufficiency. Of particular importance, the overexpression of *PKP2* in healthy cells and mice did not elicit alterations in desmosomal protein levels, nor did it induce a decline in cardiac function. These findings suggest that restoration of PKP2 levels in patients with ACM harboring a pathogenic *PKP2* mutation could lead to a therapeutic benefit.

Results

PKP2 restoration enhances CM function

In an effort to assess the relevance of PKP2 haploinsufficiency for the ACM population, we conducted a comprehensive analysis of the Dutch ACM registry (https://www.acmregistry.nl/). Of over 228 index patients from the registry, 137 (60%) have a (likely) pathogenic variant underlying their ACM phenotype[24]. Ninety-seven patients carry (likely) pathogenic *PKP2* variants. Thirty-four of these have 8 different single nucleotide substitutions in *PKP2* introducing a stop codon, originally described as c.235C>T; p.(Arg79*), c.258T>G; p.(Tyr86*), c.397C>T; p.(Gln133*), c.1848C>A; p.(Tyr616*), c.1951C>T; p.(Arg651*), c.2028G>A; p.(Trp676*), c.2203C>T; p.(Arg735*), c.2421C>A p.(Tyr807*)[25]. These findings highlight the importance of *PKP2* mutations, particularly nonsense mutations, in the pathogenesis and advancement of the disease.

To start examining the effects of PKP2 restoration in a human-relevant cell model, we utilized a patient-derived iPS cell line, harboring the pathogenic mutation *PKP2* c.2013delC (*PKP2*$^{c.2013delC/WT}$) and generated isogenic control cells as a reference[20]. To determine a suitable dosage, we delivered two different viral loads (v.l.) (v.l.1 = 0.5×10^3 viral genomes (v.g.) per cell, v.l.2 = 5×10^3 v.g. per cell) of an AAV6 vector expressing the wild-type human *PKP2* gene under the control of a cytomegalovirus (CMV) immediate-early promoter (AAV6–PKP2) (Fig. 1a). Molecular analysis of the transduced iPS-cell-derived CMs revealed a load-dependent response in PKP2 protein levels, while transduction with 5×10^3 v.g. per cell resulted in complete restoration of the PKP2 protein levels in the mutant CMs (Fig. 1c,d). To assess the effect of PKP2 restoration on desmosomal integrity, we next transduced the *PKP2* mutant iPS-cell-derived CMs with either AAV6–PKP2 or an empty AAV6 vector (AAV6-ctr) and performed mRNA and protein analysis at 4 days and 7 days post-infection, respectively (Fig. 1b). As a reference, we also treated the *PKP2*-corrected iPS-cell-derived CMs with an equal titer of the AAV6-ctr construct. Real-time polymerase chain reaction (PCR) analysis did not show any effects of the exogenously delivered *PKP2* on the mRNA expression levels of other desmosomal components, including JUP, DSP, DSG2 and DSC2 (Extended Data Fig. 1a–e). In contrast, western blot analysis revealed that restoration of PKP2 protein levels induced subsequent recovery of the desmosomal proteins, JUP and DSP, in the AAV6–PKP2-treated *PKP2*$^{c.2013delC/WT}$ iPS-cell-derived CMs, while the DSC2 and DSG2 protein levels remained unaffected (Fig. 1e–j). Performing these experiments in additional iPS-cell-derived CM lines harboring a different pathogenic *PKP2* mutation, *PKP2* c.1854C>T (*PKP2*$^{c.1854C>T/WT}$) corroborated these findings, showing rescue of desmosomal protein content in response to viral delivery of human (h)*PKP2* (Extended Data Fig. 2a–d). Together, these results indicated that restoration of physiological levels of PKP2 protein improved desmosomal assembly in human CMs harboring *PKP2* truncating variants.

As severe ventricular arrhythmia is the hallmark of ACM, we then assessed whether our 2D in vitro model recapitulates the arrhythmic substrate caused by ion channel irregularities reported to be present in other relevant studies[26,27]. We, therefore, conducted high-throughput automated patch clamp on iPS-cell-derived CMs to evaluate sodium currents (Fig. 2a). Our study included four distinct conditions, with each experiment conducted on two separate differentiations of CMs.

In comparing sodium conduction between the mutant *PKP2* CM line and the isogenic control line we were able to demonstrate a significant reduction in sodium conduction in the mutant CMs, thus successfully replicating the arrhythmic substrate characteristic of ACM (Fig. 2b,c). We subsequently sought to assess the potential of the AAV6–PKP2 gene replacement approach to ameliorate this sodium conduction impairment in the mutant CMs. Our data reveal that treatment with AAV6–PKP2 effectively diminished the differences in sodium conduction, restoring it to a level comparable to that of the isogenic control line (Fig. 2d–f).

https://doi.org/10.1038/s44161-023-00378-9

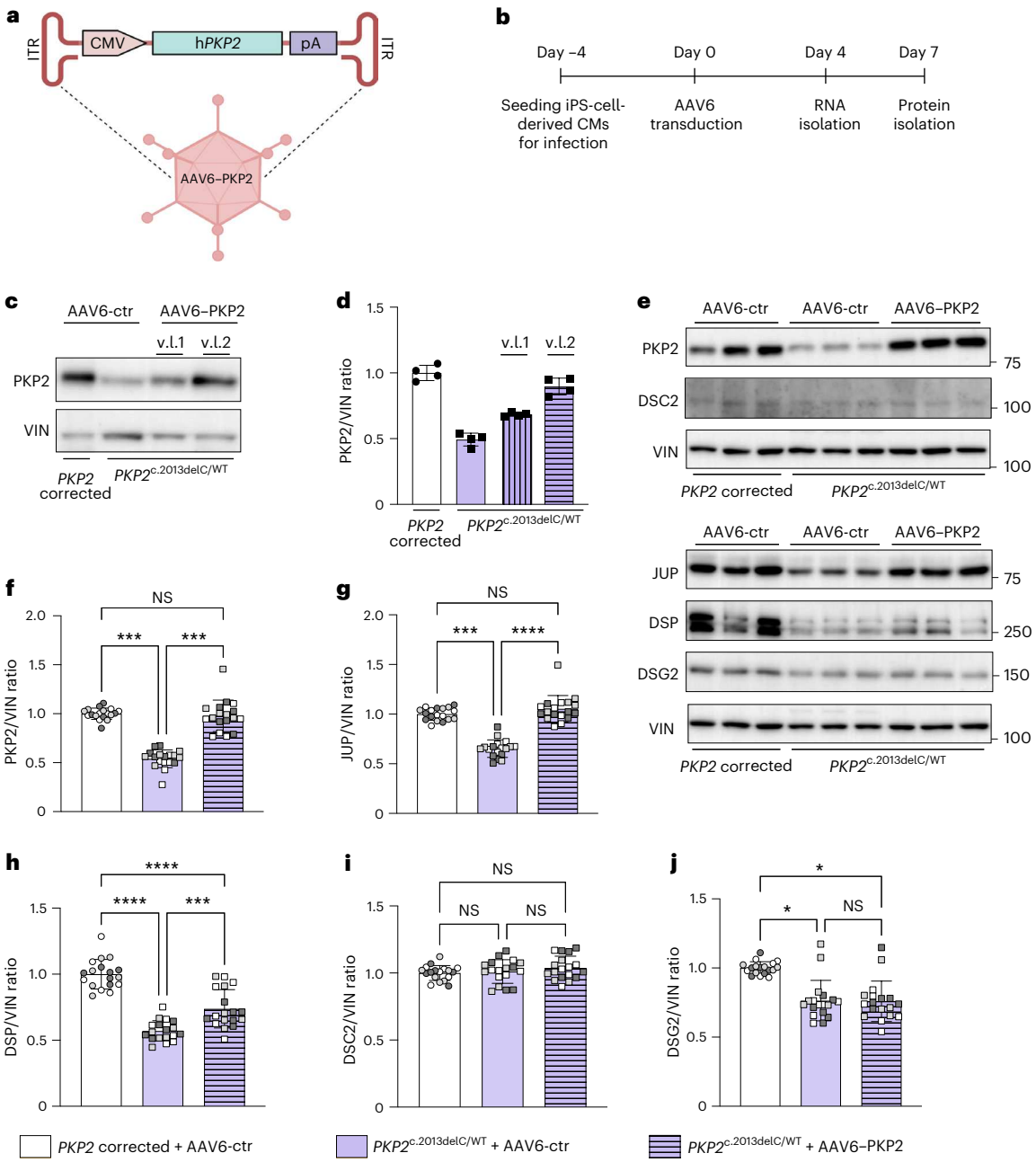

Fig. 1 | AAV-mediated restoration of PKP2 in *PKP2*$^{c.2013delC/WT}$ mutant iPS-cell-derived CMs results in molecular rescue of desmosomal assembly. **a**, Graphical representation of the AAV expression cassette used in iPS-cell-derived CMs. ITR, Inverted Terminal Repeat Sequences. **b**, Timeline for AAV6–PKP2 transduction of iPS-cell-derived CMs. **c**, Representative immunoblots showing v.l.-dependent PKP2 protein levels in *PKP2*$^{c.2013delC/WT}$ mutant cells in response to AAV6-PKP2. v.l.1 = 0.5×10^3 v.g. per cell, v.l.2 = 5×10^3 v.g. per cell. Vinculin (VIN) was used as a loading control. **d**, Quantification of **c**, $n = 4$ technical replicates per condition. **e**, Representative immunoblots for PKP2, JUP, DSP, DSG2 and DSC2 in corrected and mutant iPS-cell-derived CMs upon transduction with AAV6-ctr or AAV6–PKP2. VIN was used as a loading control. **f**, Quantification of PKP2 protein levels. **g**, Quantification of JUP protein levels. **h**, Quantification of DSP protein levels. **i**, Quantification of DSC2 protein levels. **j**, Quantification of DSG2 protein levels. Colored dots represent distinct CM differentiation, $n = 6$ technical replicates and 3 biological replicates per condition. Data is presented as mean values ± s.e.m. Statistical significance is derived from biological replicates and determined with one-way ANOVA (Tukey's post-hoc test), *P* value at $^{****}P < 0.0001$, $^{***}P < 0.001$, $^{**}P < 0.01$, $^{*}P < 0.05$, and not significant (NS). *P* values (from left to right): 0.0003, 0.91, 0.0004 (**f**); 0.0002, 0.3778, <0.0001 (**g**); <0.0001, <0.0001, 0.0007 (**h**); 0.0138, 0.0125, 0.9955 (**j**).

These findings show that a gene replacement approach improves sodium conduction in mutant CMs, which might suggest it could rescue the arrhythmic phenotype in patients with ACM.

PKP2 restoration enhances contractile function in engineered human myocardium

As PKP2 plays a major role in intercellular binding and interaction, we next generated three-dimensional (3D) EHM composed of 70% iPS-cell-derived CMs combined with 30% human foreskin fibroblasts (HFFs) in a collagen type I-based hydrogel (Fig. 3a and Extended Data Fig. 3a,b). This model provides a more mature CM phenotype compared to 2D cell cultures, while enabling the sequential assessment of contractile properties at various stages of tissue maturation[28].

Interestingly, *PKP2*$^{c.2013delc/WT}$ tissues exhibited a significant reduction in expression of cardiac markers, including α-actinin-2 (*ACTN2*) accompanied by an increase in the expression levels of several fibroblast

https://doi.org/10.1038/s44161-023-00378-9

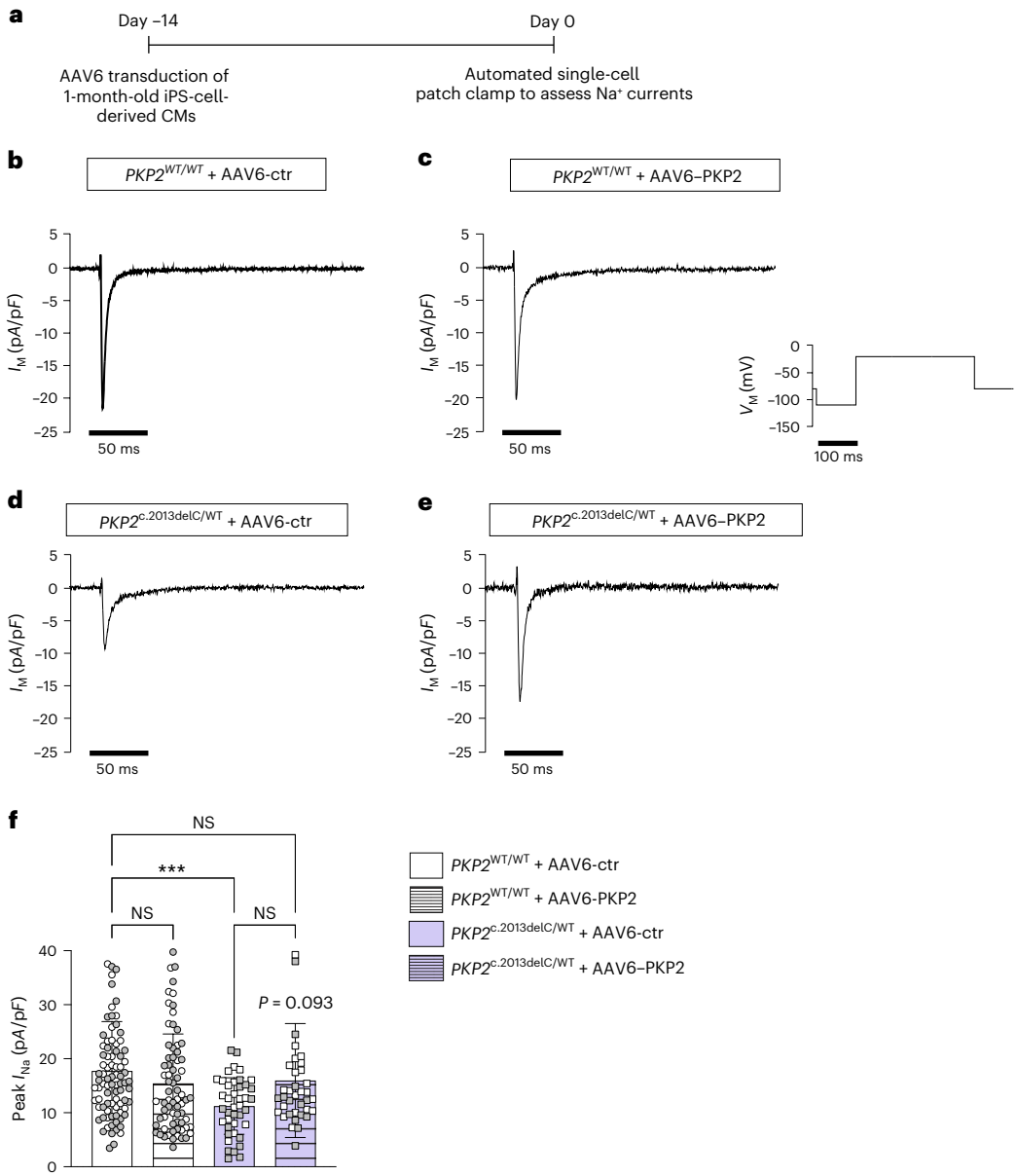

Fig. 2 | AAV-mediated restoration of PKP2 in *PKP2*$^{c.2013delC/WT}$ mutant iPS-cell-derived CMs improves sodium conduction. a, Graphical representation of the experimental workflow. **b**–**e**, Representative voltage-gated sodium currents activated by voltage steps to between −80 mV and −20 mV from a holding potential of −110 mV. Experimental groups: *PKP2*$^{WT/WT}$ + AAV6-ctr shown in **b**, *PKP2*$^{WT/WT}$ + AAV6-PKP2 shown in **c**, *PKP2*$^{c.2013delC/WT}$ + AAV6-ctr shown in **d**, *PKP2*$^{c.2013delC/WT}$ + AAV6-PKP2 shown in **e**. **f**, Graph showing the peak transient I_{Na} density for each experimental group. Colored dots represent distinct CM differentiation. *PKP2*$^{WT/WT}$ + AAV6-ctr: n = 39 single CMs (diff.1) + 48 single CMs (diff.2), *PKP2*$^{WT/WT}$ + AAV6–PKP2: n = 26 single CMs (diff.1) + 44 single CMs (diff.2), *PKP2*$^{c.2013delC/WT}$ + AAV6-ctr: n = 21 single CMs (diff.1) + 20 single CMs (diff.2), *PKP2*$^{c.2013delC/W}$ + AAV6–PKP2: n = 23 single CMs (diff.1) + 14 single CMs (diff.2). Data are presented as mean values ± s.e.m. Statistical significance was estimated with one-way ANOVA, Tukey correction with P value at $^{****}P < 0.0001$, $^{***}P < 0.001$, $^{**}P < 0.01$, $^{*}P < 0.05$, and not significant (NS). P values (**f**): *PKP2*$^{WT/WT}$ + AAV6-ctr versus *PKP2*$^{c.2013delC/WT}$ + AAV6-ctr = 0.0008; *PKP2*$^{c.2013delC/WT}$ + AAV6-ctr versus *PKP2*$^{c.2013delC/WT}$ + AAV6–PKP2 = 0.0930; *PKP2*$^{WT/WT}$ + AAV6-ctr versus *PKP2*$^{c.2013delC/WT}$ + AAV6–PKP2 = 0.7177.

markers such as vimentin (*VIM*) and decorin (*DCN*) compared to the isogenic control (Extended Data Fig. 3c). Furthermore, the mutant tissues showed significantly higher levels of the stress-related gene *NPPB* (Extended Data Fig. 3c). Notably we did not detect the presence of fibrofatty markers in either of the two genotypes. Despite these transcriptional differences, our histological examination using Masson's trichrome staining did not reveal substantial differences in fibrosis between the two genotypes at the tissue level (Extended Data Fig. 3d,e). Immunofluorescence assays on 6-week-old EHM revealed colocalization of PKP2 with the ID-specific marker N-cadherin (NCAD), however a more organized ID-like structure was more evident in the control tissues compared to the mutant tissues (Extended Data Fig. 3f). These results suggest that both the *PKP2* mutant and isogenic control EHM develop a myocardium-like structure, albeit with differences in the organization of CM junctions, which appear to be improved in both lines compared to the 2D cultures.

Next, we sought to investigate the desmosomal composition of the mutant and isogenic control EHM. Molecular analysis by western blot confirmed a two-fold decline of PKP2 protein levels in *PKP2*$^{c.2013delC/WT}$ EHM compared to *PKP2*$^{WT/WT}$ EHM, accompanied by a reduction in JUP and DSP protein levels, which is consistent with the molecular phenotype observed in 2D cultures (Fig. 3b,d–f). The desmosomal

https://doi.org/10.1038/s44161-023-00378-9

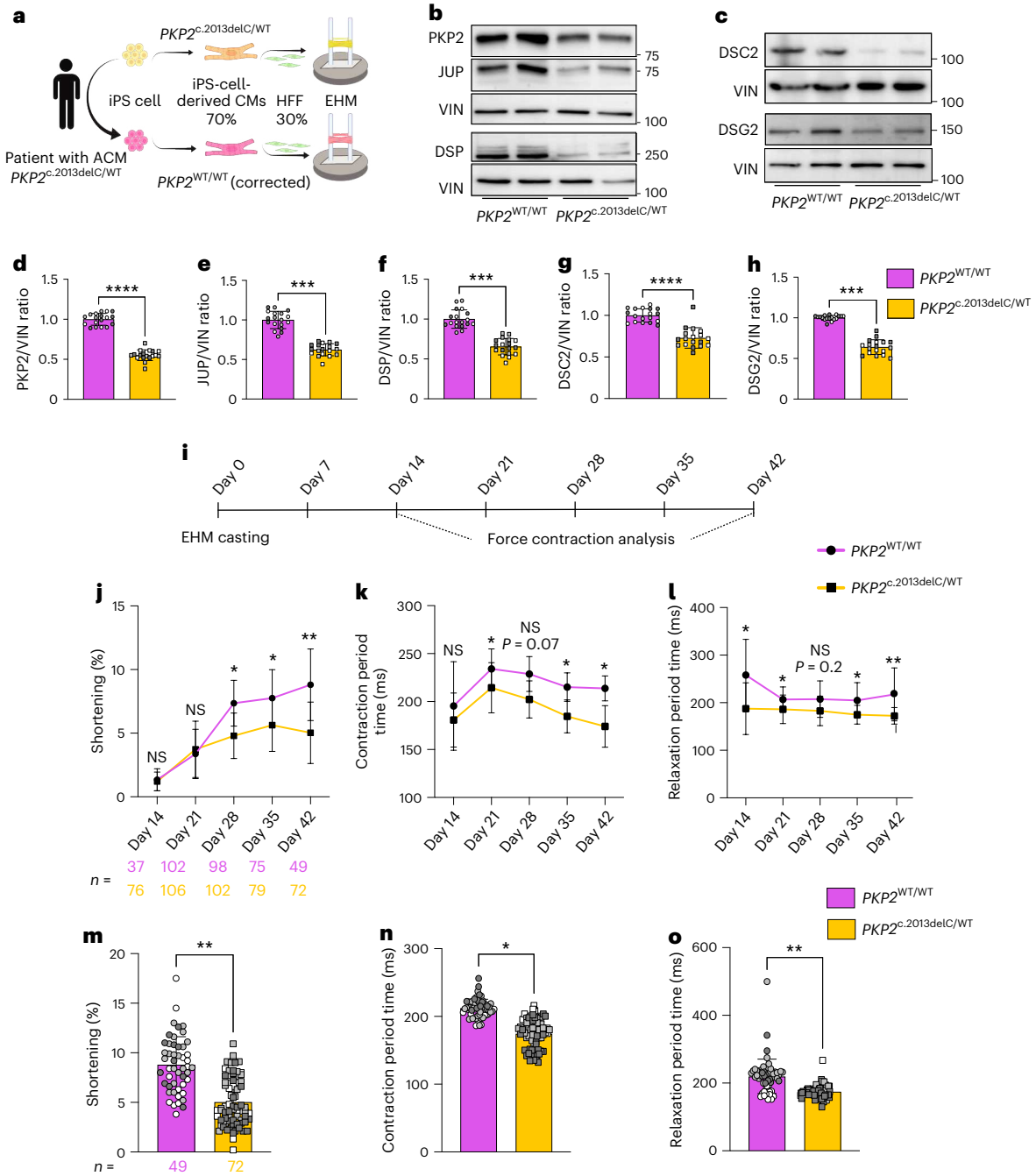

Fig. 3 | *PKP2*$^{c.2013delC/WT}$ mutant EHM exhibit impaired contractile function compared to the isogenic control. a, Schematic overview of the generation of *PKP2* EHM. **b**, Representative immunoblot for the desmosomal proteins PKP2, JUP and DSP. VIN is used as a loading control. **c**, Representative immunoblot for the desmosomal proteins DSC2 and DSG2. VIN is used a loading control. **d**, Quantification of PKP2 protein levels. **e**, Quantification of JUP protein levels. **f**, Quantification of DSP protein levels. **g**, Quantification of DSC2 protein levels. **h**, Quantification of DSG2 protein levels. Colored dots represent distinct CM differentiations, $n = 6$ technical replicates and 3 biological replicates per condition. Data are presented as mean values ± s.e.m. Statistical significance is derived by biological replicates and determined by unpaired, two-tailed Student's *t*-test, *P* value at $^{****}P < 0.0001$, $^{***}P < 0.001$, $^{**}P < 0.01$, $^{*}P < 0.05$, and not significant (NS). **i**, Timeline for assessing contractility of *PKP2*$^{WT/WT}$ and *PKP2*$^{c.2013delC/WT}$ EHM. **j**, Trendline showing % pole bending as a measure of force of contraction for *PKP2*$^{WT/WT}$ and *PKP2*$^{c.2013delC/WT}$ EHM under baseline conditions at different time points. **k**, Trendline showing contraction time (from 20% to 80% contraction in ms) for *PKP2*$^{WT/WT}$ and *PKP2*$^{c.2013delC/WT}$ EHM under baseline condiitons at different time points. **l**, Trendline showing relaxation time (from 20% to 80% relaxation in ms) for *PKP2*$^{WT/WT}$ and *PKP2*$^{c.2013delC/WT}$ EHM under baseline conditions at different time points. Statistics: one-way ANOVA with Tukey's post-hoc test was performed between all groups at each time point, $n = 3$ biological replicates (exact number for technical replicates is indicated on the figure). **m**, Graph displaying force of contraction (as % pole bending) for *PKP2*$^{WT/WT}$ and *PKP2*$^{c.2013delC/WT}$ EHM on day 42 of maturation. **n**, Graph displaying contraction time (ms) for *PKP2*$^{WT/WT}$ and *PKP2*$^{c.2013delC/WT}$ EHM on day 42 of maturation. **o**, Graph displaying relaxation time (ms) for *PKP2*$^{WT/WT}$ and *PKP2*$^{c.2013delC/WT}$ EHM on day 42 of maturation. Colored dots represent distinct CM differentiations, $n = 3$ biological replicates (*PKP2*$^{WT/WT}$ EHM: $n = 17$ (diff.1), 21 (diff.2) and 11 (diff.3) technical replicates. *PKP2*$^{c.2013delC//WT}$ EHM: $n = 19$ (diff.1), 23 (diff.2) and 30 (diff.3) technical replicates). Data are presented as mean values ± s.e.m. Statistical significance is derived from biological replicates and determined by unpaired, two-tailed Student's *t*-test, *P* value at $^{****}P < 0.0001$, $^{***}P < 0.001$, $^{**}P < 0.01$, $^{*}P < 0.05$, and not significant (NS). *P* values: 0.0002 (**d**), <0.0001 (**e**), 0.010 (**f**), <0.0001 (**g**), 0.0003 (**h**), 0.095 (42-day time point) (**j** and **m**), 0.0176 (42-day time point) (**k** and **n**) and 0.059 (42-day time point) (**l** and **o**).

cadherins DSC2 and DSG2 also showed reduced protein levels in the mutant tissues compared to the control tissues, which for DSC2 was not observed in our 2D model (Figs. 1i and 3c,g–h). This discrepancy might be attributed to the different levels of maturation that the two models present. It is also possible that the mechanical stress that is involved in EHM culture exacerbates the overall phenotype observed, therefore leading to a decline of DSC2 protein. In parallel, video-optical recordings of EHM contraction revealed a significant decline in contractile function (decrease in force of contraction) in *PKP2* mutant EHM compared to the *PKP2*$^{WT/WT}$ EHM (Fig. 3i–o). Other contractility properties, including beating frequency, contraction velocity and relaxation velocity, did not show significant differences between mutant and isogenic control tissues throughout maturation (Extended Data Fig. 4a–g).

To determine whether PKP2 restoration could improve the functional phenotype observed in mutant tissues, we transduced *PKP2*$^{c.2013delC/WT}$ and *PKP2*$^{WT/WT}$ iPS-cell-derived CMs with either the AAV6–PKP2 or the AAV6-ctr and reconstituted the CMs to EHM 3 days post-transduction (Fig. 4a,b). Our results showed successful PKP2 restoration in the *PKP2*$^{c.2013delC/WT}$–AAV6–PKP2 tissues at 6 weeks after EHM formulation, which was paralleled by a strong increase in JUP, DSP and DSG2 protein levels (Fig. 4c–g). Interestingly, DSC2 protein levels did not respond to PKP2 restoration (Extended Data Fig. 5a,b). Apart from the desmosomal proteins, we also assessed the levels of other ID-related factors including NCAD and αCAT. PKP2 restoration was sufficient to restore the levels of these proteins in the mutant tissues, potentially implying that a stronger junction is formed between the adjacent CMs (Fig. 4c,h,i). Importantly, *PKP2* overexpression in the *PKP2*$^{WT/WT}$ tissues did not lead to a significant increase in PKP2 or other desmosomal protein levels, potentially implying that an excess of PKP2 is being degraded by the cellular housekeeping machinery.

At a functional level, AAV6–PKP2 transduction resulted in a progressive improvement in contraction amplitude and normalization of the altered contraction kinetics, that is, an elongation of contraction and relaxation duration towards *PKP2*$^{WT/WT}$ levels in the *PKP2*$^{c.2013delC/WT}$ EHM from day 28, reaching statistical significance on day 42 post-casting (Fig. 4j–o). Noteworthily, *PKP2* expression in the AAV6–PKP2-treated isogenic control EHM did not lead to any side effects on the contractile phenotype, further supporting our hypothesis that *PKP2* overexpression is not detrimental to healthy CMs.

These data show that AAV-mediated restoration of PKP2 leads to molecular and functional benefits in ACM–EHM models with PKP2 haploinsufficiency.

In vivo PKP2 delivery restores CM junctions

To further increase clinical relevance, we made use of our previously described murine ACM model, harboring the mouse equivalent of the human pathogenic *PKP2* c.2013delC variant (*Pkp2*$^{c.1755delA/WT}$). In brief, the *Pkp2*$^{c.1755delA/WT}$ mice exhibit a significant reduction of cardiac desmosomal and adherens junction protein levels compared to *Pkp2*$^{WT/WT}$ mice[20]. To administer *Pkp2* in vivo, we generated an AAV9 vector overexpressing the murine wild-type *Pkp2* fused to a MYC epitope to enable detection of the exogenously delivered PKP2 (AAV9–PKP2) (Fig. 5a). As a proof of concept, we initially administered an AAV9–PKP2 dose of 2×10^{14} v.g. kg^{-1} via intraperitoneal injections (IP) on 5-day-old *Pkp2* mutant pups and their wild-type control, and collected tissues 2 weeks after injection (Fig. 5b). Efficiency of transduction was approximately 76% of CMs (Supplementary Fig. 6a,b). Immunohistochemistry on paraffin sections of the murine hearts revealed correct localization of the exogenous PKP2 within the IDs, indicating functionality of the exogenous protein (Fig. 5c). Immunoblot analysis showed successful restoration of PKP2 protein levels in the treated mutant mice, corresponding to a significant recovery of JUP and a partial recovery in DSP and DSG2 (Fig. 5d–i), whereas DSC2 was not responsive to different PKP2 levels (Extended Data Fig. 7a, b). These findings are in line with what has been observed in our EHM models, consistently indicating the re-building of the desmosomal complex upon PKP2 restoration in our preclinical ACM models.

Since ACM symptoms often become apparent during early adulthood, we investigated the effect of AAV9–PKP2 administration at a more clinically relevant stage. For this purpose, we intravenously injected *Pkp2* mutant and wild-type mice at 2 months of age with a dose of 5×10^{13} v.g. kg^{-1} of either AAV9–PKP2 or AAV9-ctr (efficiency of transduction: 71% CMs in the left ventricle (LV)). Two weeks later we isolated tissues for molecular analysis (Fig. 5j). PKP2 restoration in the mutant mice resulted in elevated levels of the desmosomal proteins, JUP, DSP and DSG2, whereas DSC2 did not show an increase (Fig. 5k,l–o and Extended Data Fig. 7c,d). Importantly, PKP2 restoration also led to a significant recovery of adherens junction proteins, including NCAD and α-CAT, in line with what we observed on the EHM models (Fig. 4c,h,i). These results point to the formation of stronger junctions in the CMs of *Pkp2* mutant mice injected with AAV9–PKP2 and further support the therapeutic potential of PKP2 restoration in patients with ACM.

PKP2 restoration improves cardiac function in mice

To assess the consequences of long-term *Pkp2* administration on cardiac function in vivo, we injected both wild-type and mutant 2-month-old mice with a single dose (3×10^{13} v.g. kg^{-1}) of either AAV9-ctr or

Fig. 4 | AAV-mediated restoration of PKP2 in *PKP2*$^{c.2013delC/WT}$ EHM leads to an increase in desmosomal and junctional protein levels, which further translates into improved contractility. a, Timeline for the AAV transduction and maturation of *PKP2*$^{WT/WT}$ and *PKP2*$^{c.2013delC/WT}$ EHM with either AAV6-ctr or AAV6–PKP2. **b**, Representative fluorescent image of 6-week-old EHM transduced with either AAV6-ctr (left) or AAV6–PKP2 fused with the mNeongreen fluorescent protein (right). Scale bar, 1 mm. This experiment was repeated independently three times with similar results. **c**, Representative immunoblots for PKP2, JUP, DSP, DSG2, NCAD and αCAT in 6-week-old *PKP2*$^{WT/WT}$ and *PKP2*$^{c.2013delC/WT}$ EHM, transduced either with AAV6-ctr or AAV6–PKP2. VIN was used as a loading control for the desmosomal proteins, whereas αTUB was used for the quantification of NCAD and αCAT. **d**, Quantification of PKP2 protein levels. **e**, Quantification of JUP protein levels. **f**, Quantification of DSP protein levels. **g**, Quantification of DSG2 protein levels. **h**, Quantification of NCAD protein levels. **i**, Quantification of αCAT protein levels. Colored dots represent distinct CM differentiations, $n = 6$ technical replicates and 3 biological replicates per condition. Data are presented as mean values ± s.e.m. Statistical significance is derived from biological replicates and determined by one-way ANOVA (Tukey's post-hoc test), P value at $^{****}P < 0.0001$, $^{***}P < 0.001$, $^{**}P < 0.01$, $^{*}P < 0.05$, and not significant (NS). **j**, Trendline showing % pole bending as a measure of force of contraction for *PKP2*$^{WT/WT}$ and *PKP2*$^{c.2013delC/WT}$ EHM after AAV6 transduction at different time points. **k**, Trendline showing contraction time (from 20% to 80% contraction in ms) for *PKP2*$^{WT/WT}$ and *PKP2*$^{c.2013delC/WT}$ EHM after AAV6 transduction at different time points. **l**, Trendline showing relaxation time (from 20% to 80% relaxation in ms) for *PKP2*$^{WT/WT}$ and *PKP2*$^{c.2013delC/WT}$ EHM after AAV6 transduction at different time points. Statistics: one-way ANOVA with Tukey's post-hoc test was performed between all groups at each time point, $n = 3$ biological replicates and 36 technical replicates per condition (12 tissues per CM differentiation). **m**, Graph summarizing force of contraction (% pole bending) for *PKP2*$^{WT/WT}$ and *PKP2*$^{c.2013delC/WT}$ EHM on day 42 of maturation. **n**, Graph summarizing contraction time (ms) for *PKP2*$^{WT/WT}$ and *PKP2*$^{c.2013delC/WT}$ EHM on day 42 of maturation. **o**, Graph summarizing relaxation time (ms) for *PKP2*$^{WT/WT}$and *PKP2*$^{c.2013delC/WT}$ EHM on day 42 of maturation, $n = 3$ biological replicates and 36 technical replicates (12 tissues per condition). Data are presented as mean values ± s.e.m. Statistical significance is derived from biological replicates and determined by one-way ANOVA (Tukey's post-hoc test), P value at $^{****}P < 0.0001$, $^{***}P < 0.001$, $^{**}P < 0.01$, $^{*}P < 0.05$, and not significant (NS). P value (*PKP2*$^{c.2013delC/WT}$ + AAV6-ctr versus *PKP2*$^{c.2013delC/WT}$ + AAV6–PKP2): 0.0010 (**d**), 0.0006 (**e**), 0.3638 (**f**), <0.0001 (**g**), 0.3156 (**h**), <0.0001 (**i**), 0.0033 (**j** and **m**), 0.0274 (**k** and **n**) and 0.0344 (**l** and **o**).

https://doi.org/10.1038/s44161-023-00378-9

AAV9–PKP2 and monitored heart function at 4, 8 and 12 months of age (Fig. 6a). We aged the mice up to 12 months as the mutant mice show progressive cardiac dysfunction with age, showing a significant decrease in the ratio of the early (E) to late (A) ventricular filling velocities (E/A ratio) and a significant increase in isovolumic relaxation time (IVRT) compared to the wild-type mice[20]. Ten months after a single injection, immunohistochemistry indicated the presence of exogenous PKP2 at the IDs of 12-month-old mouse hearts (Fig. 6b and

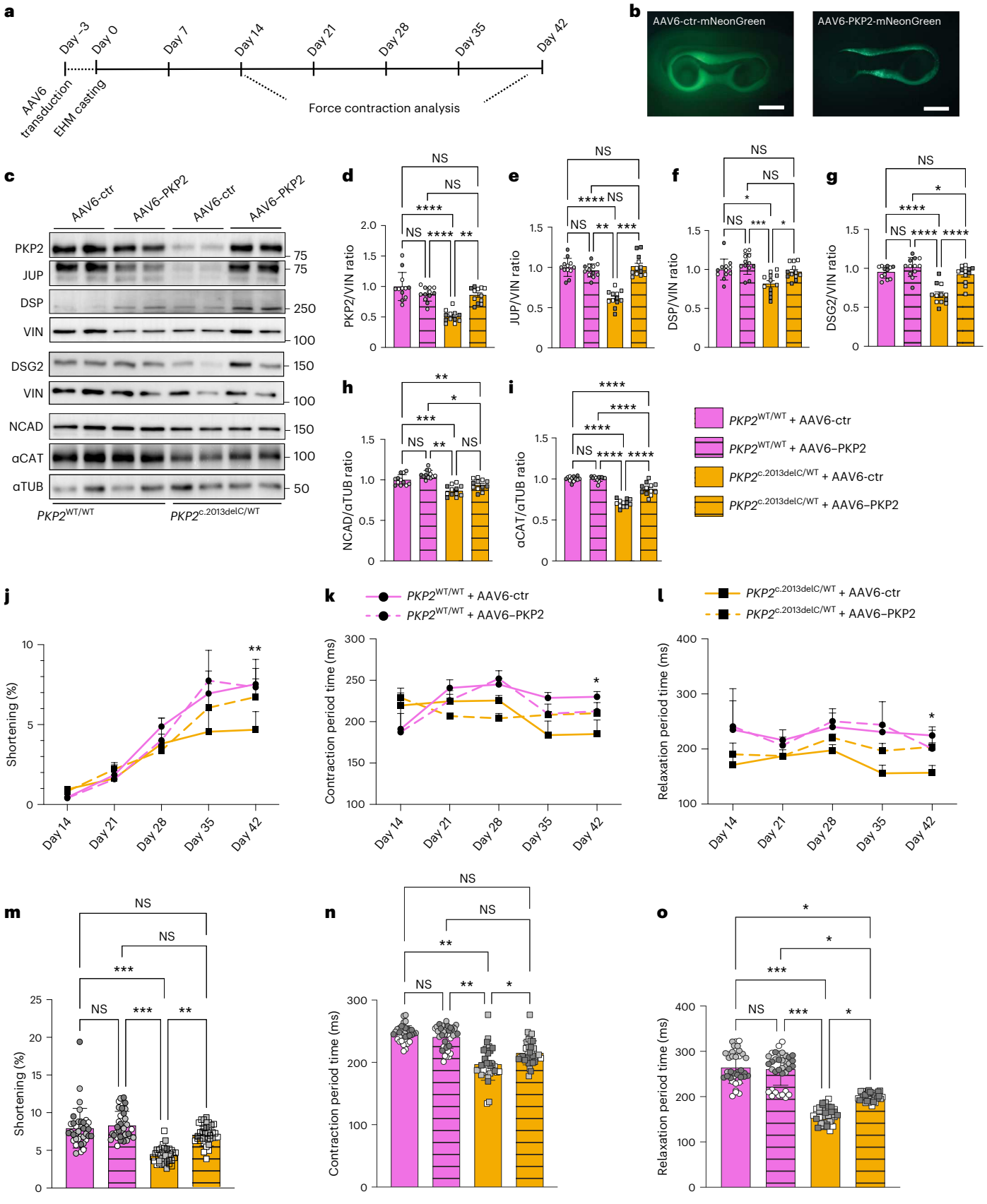

Extended Data Fig. 8). Western blot analysis of the hearts extracted from AAV9–PKP2-treated mutant mice demonstrated restoration of the PKP2 protein levels and a significant recovery of the desmosomal proteins JUP, DSP and DSG2 including also DSC2 which was not responsive in the more immature models (Fig. 6c–h and Extended Data Fig. 7e,f). Interestingly, in line with our observations in the *PKP2*$^{WT/WT}$ EHM, wild-type mice injected with the AAV9–PKP2 virus did not show a significant increase in PKP2 levels and also the protein levels of the assessed desmosomal components remained unaltered. In accordance with our previous study, echocardiographic analysis at baseline, 4 months, 8 months and 12 months of age did not reveal any significant differences in ejection fraction (EF) (Fig. 6i), LV mass, LV end diastolic volume (LVEDV) and LV end systolic volume (LVESV) between mutant and wild type (Extended Data Fig. 9a–e). Long-term exposure to either AAV-ctrl or AAV–PKP2 did also not influence these cardiac functional and morphological measures, further supporting that *Pkp2* overexpression does not impair cardiac physiology (Extended Data Fig. 9a–e). Importantly, assessment of E/A ratio and IVRT at the 12-month time point revealed a significant improvement in the AAV9–PKP2-treated mutant mice compared to the mutant mice injected with the AAV9-ctr (Fig. 6j,k). These data suggest that *Pkp2* administration in the mutant mice reinstates physiological gene expression profiles, improves electrical and mechanical coupling and eventually restores cardiac function. Morphological evaluation did not demonstrate significant differences in heart weight/body weight and heart weight/tibia length ratio among the different experimental groups (Extended Data Fig. 9e,f). Moreover, protein analysis of tissues that are prone to receive AAV9–PKP2 particles including lung, liver, spleen and kidney showed moderate expression of the exogenous PKP2 within the liver, which could be explained by the high liver tissue tropism of AAVs[29] (Extended Data Fig. 6c–e). Overall, these data indicate that a single dose of AAV9–PKP2 is able to rescue the molecular and functional phenotype observed in the *Pkp2*$^{c.1755delA/WT}$ adult mice without causing overt adverse effects in the heart and other organs.

Discussion

PKP2 haploinsufficiency is often the underlying cause for ACM[13]. The data presented in this manuscript underscore the therapeutic potential of *PKP2* gene replacement therapy by showing both molecular and functional rescue in human-relevant preclinical in vitro and in vivo models of ACM, with no apparent detrimental effects of *PKP2* overexpression under healthy conditions. These are important findings that support the exploration of *PKP2* gene therapy as a targeted therapeutic treatment option for patients suffering from ACM.

Our data show that *PKP2* replacement under conditions of PKP2 haploinsufficiency can restore desmosomal integrity and CM function. These results are in line with a prior study by Inoue et al. that demonstrated AAV2-mediated PKP2 restoration in PKP2-deficient iPS-cell-derived CMs to restore other desmosomal components and enhance contractility[30]. By treating *PKP2*$^{c.2013delC/WT}$ EHM with AAV6–PKP2 we were also able to show that the functional improvement is longlasting and progressive since the treated tissues showed constant improvement in contractile function from day 28 until day 42 post casting. Moreover, *PKP2* overexpression under healthy conditions did not appear to influence desmosomal integrity or CM function, which would be an important safety parameter for moving this technology into patients.

Next to our in vivo efficacy data, we provide evidence that a single systemic administration of AAV9–PKP2 in heterozygous mice harboring a pathogenic *PKP2* variant leads to restoration of desmosomal assembly in the transduced CMs, which is accompanied by the recovery of intercellular junction proteins NCAD and α-CAT. In time, *PKP2* gene therapy also prevents diastolic dysfunction in treated mutant mice at 12 months of age, while showing no effect in healthy wild-type littermates. This might be due to the lack of excessive PKP2 levels in both our wild-type in vitro and in vivo models. The lack of overexpression under healthy conditions might suggest the presence of a cellular compensatory mechanism correcting for an overdose of PKP2 protein. Similar observations have been reported for the exogenous expression of sarcomere genes in CMs. It has been demonstrated that viral expression of the hypertrophic cardiomyopathy-associated sarcomere gene myosin binding protein C (*MYBPC3*), can lead to the replacement of the endogenous protein without overexpression. This is due to UPS-mediated degradation of the excess amount of sarcomere proteins to preserve the stoichiometry of the sarcomere complex[31–33]. So far it is unclear whether UPS-mediated protein degradation also plays a role in maintaining PKP2 protein at physiological levels in CMs. While here we show therapeutic benefit in a mutant *Pkp2* mouse model, another recent study utilized gene therapy to correct the arrhythmic phenotype observed in a mouse model of ACM carrying a homozygous knock-in variant in the *Dsg2* gene (*Dsg2*$^{-/-}$)[34]. The authors were able to rescue the arrhythmic but not the fibrotic phenotype in the mutant mice, by AAV9-mediated administration of the truncated isoform of CX43 (*GJA1-20k*), which is responsible for correct localization of CX43 at the IDs.

In this study, we used murine models of PKP2 haploinsufficiency harboring the mouse equivalent of the known pathogenic mutation *PKP2* c.2013delC to mimic the genetic condition of patients. However, there are significant differences between the electrophysiological properties of hearts of human and mice[35]. For example, mouse hearts have weaker Ca^{2+} currents and stronger K^+ currents[36] resulting in a shorter ventricular action potential duration and a heart rate about ten times higher than in humans. These differences, including the sparsity of detectable T-waves in mouse hearts[37], complicate the identification of cardiac defects in our models.

Fig. 5 | AAV-mediated restoration of PKP2 in *Pkp2*$^{c.1755delA/WT}$ pups and adult mice leads to the recovery of desmosomal and non-desmosomal components of the ID. a, Graphical representation of the AAV expression cassette used in mice, ITR=Inverted Terminal Repeat Sequences. **b**, Workflow followed after the intraperitoneal (IP) AAV9–PKP2 administration in *Pkp2*$^{c.1755delA/WT}$ and wild-type pups. **c**, Immunofluorescence on paraffin sections of mouse cardiac tissue showing localization of the exogenously introduced PKP2 in the injected hearts. DAPI, blue; ACTN2, gray; PKP2, green; MYC epitope, red; exogenous PKP2, yellow in merged image. Scale bar, 10 µm. This experiment was repeated independently 18 times (in 18 distinct mouse hearts) with the same results. **d**, Representative immunoblots for PKP2, MYC, JUP, DSP and DSG2 in *Pkp2*$^{WT/WT}$ and *Pkp2*$^{c.1755delA/WT}$ pups injected with either AAV9-ctr or AAV9–PKP2. VIN is used as a loading control. **e**, Quantification of PKP2 protein levels. **f**, Quantification of MYC protein levels. **g**, Quantification of JUP protein levels. **h**, Quantification of DSP protein levels. **i**, Quantification of DSG2 protein levels. Experimental groups: *Pkp2*$^{WT/WT}$ pups injected with AAV9-ctr $n = 8$, *Pkp2*$^{c.1755delA/WT}$ pups injected with AAV9-ctr $n = 8$, *Pkp2*$^{c.1755delA/WT}$ pups injected with AAV9–PKP2 $n = 10$. **j**, Workflow followed after the intravenous (IV) AAV9–PKP2 administration in *Pkp2*$^{c.1755delA/WT}$ and wild-type adult mice. **k**, Representative immunoblots for the desmosomal PKP2, MYC, JUP, DSP and DSG2 and NCAD and αCAT in *Pkp2*$^{WT/WT}$ and *Pkp2*$^{c.1755delA/WT}$ mice injected with either AAV9-ctr or AAV9–PKP2. VIN is used as a loading control for the desmosomal proteins, whereas GAPDH is used for the quantification of NCAD and αCAT. **l**, Quantification of PKP2 protein levels. **m**, Quantification of JUP protein levels. **n**, Quantification of DSP protein levels. **o**, Quantification of DSG2 protein levels. **p**, Quantification of MYC protein levels. **q**, Quantification of NCAD protein levels. **r**, Quantification of αCAT protein levels. Experimental groups: *Pkp2*$^{WT/WT}$ mice injected with AAV9-ctr $n = 10$, *Pkp2*$^{WT/WT}$ mice injected with AAV9–PKP2 $n = 10$, *Pkp2*$^{c.1755delA/WT}$ mice injected with AAV9-ctr $n = 10$, *Pkp2*$^{c.1755delA/WT}$ mice injected with AAV9–PKP2 $n = 10$. Data are presented as mean values ± s.e.m. Statistical significance is determined by one-way ANOVA (Tukey's post-hoc test), *P* value at $^{****}P < 0.0001$, $^{***}P < 0.001$, $^{**}P < 0.01$, $^{*}P < 0.05$, and not significant (NS). *P* value (*Pkp2*$^{c.1755delA/WT}$ + AAV9-ctr versus *Pkp2*$^{c.1755delA/WT}$ + AAV9-PKP2): <0.0001 (**e**), <0.0001 (**g**), 0.3461 (**h**), 0.1607 (**i**), 0.002 (**l**), <0.0001 (**m**), 0.029 (**n**), 0.0122 (**o**), <0.0001 (**q**) and <0.0001 (**r**).

https://doi.org/10.1038/s44161-023-00378-9

In vitro, we employed EHM as a valuable tool to study cardiac function. Nevertheless, EHM have their own set of limitations when it comes to modeling arrhythmias. Arrhythmias in ACM often coincide with the presence of abnormal collagen deposition and lipid droplets. In our *PKP2* mutant tissues, we did not observe either of these characteristics. This observation aligns with expectations since these changes typically take years to develop in patients with ACM, whereas our tissue samples were cultured for only 1 month. Additionally, it is worth noting that only the CMs in our model were patient-specific, while the cardiac fibroblasts were not. There is an ongoing debate in the scientific literature regarding whether arrhythmias are primarily driven by CMs alone or in combination with other cell types[38–40]. Many studies suggest that factors such as fibrosis, CM death and the infiltration of fibro-fatty tissue create the substrate for triggering arrhythmias[41].

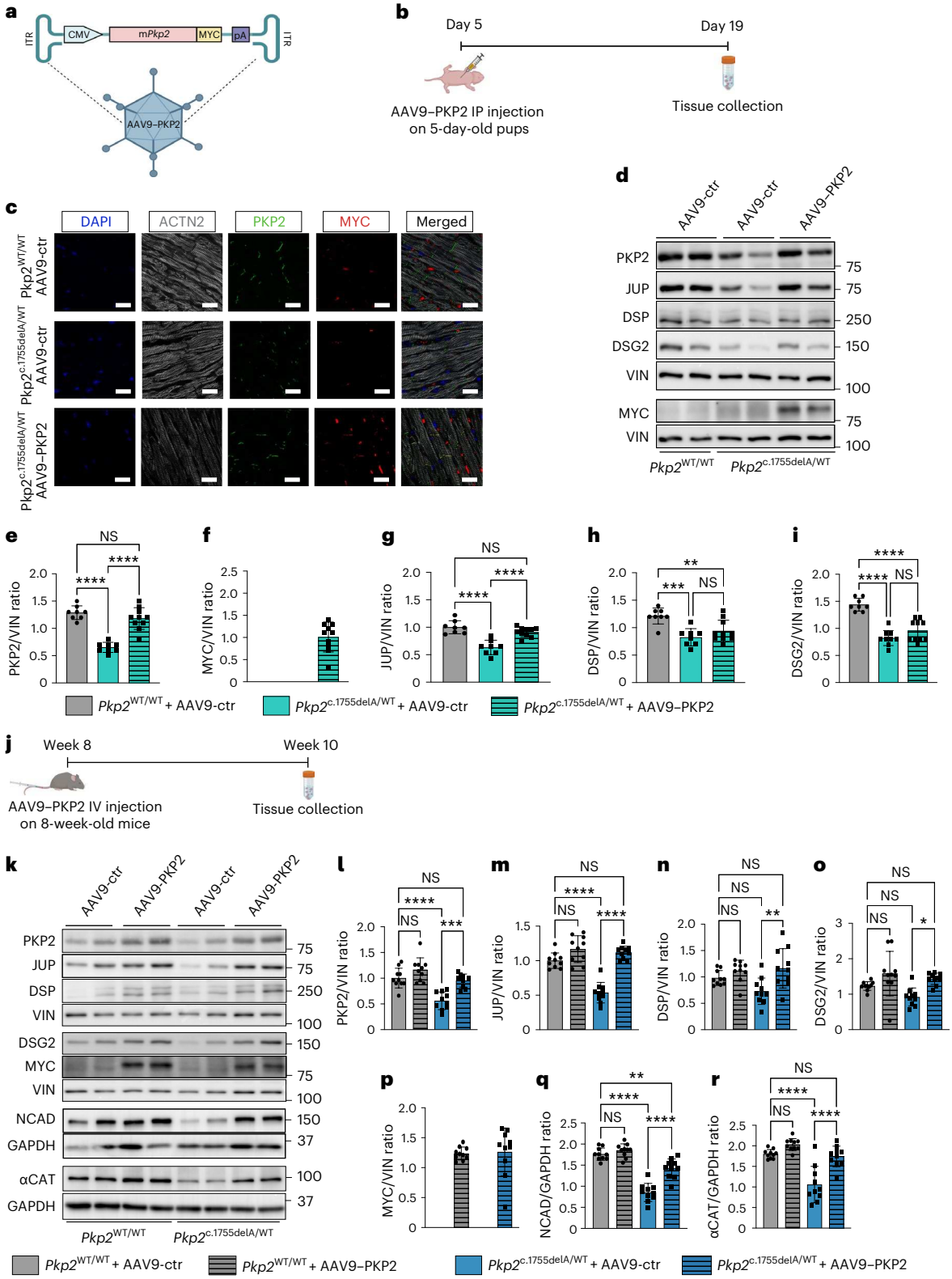

https://doi.org/10.1038/s44161-023-00378-9

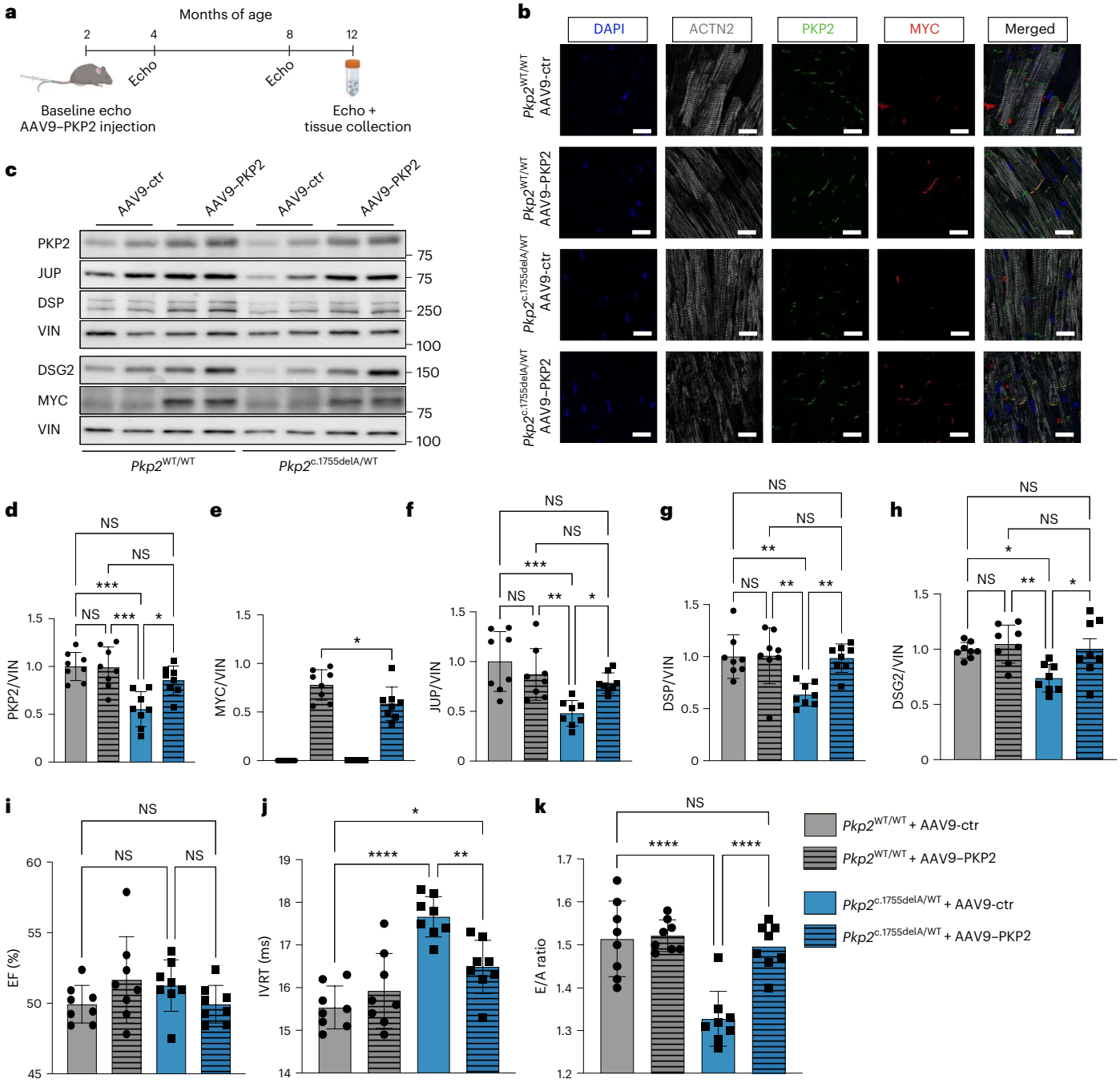

Fig. 6 | A single dose of AAV9-PKP2 in 8-week-old *Pkp2*$^{c.1755delA/WT}$ mice prevents cardiac dysfunction at 12 months of age. a, Timeline for intravenous AAV9–PKP2 administration in *Pkp2*$^{c.1755delA/WT}$ and long-term monitoring of cardiac function in adult mice. **b**, Immunofluorescence on paraffin sections of mouse cardiac tissue showing localization of the exogenously introduced PKP2 in the injected hearts. DAPI, blue; ACTN2, gray; PKP2, green; MYC epitope, red; exogenous PKP2, yellow in merged image. Scale bar, 10 µm. This experiment was performed independently ten times (in ten distinct mouse hearts) with the same results. **c**, Representative immunoblots for PKP2, MYC, JUP, DSP and DSG2 in *Pkp2*$^{WT/WT}$ and *Pkp2*$^{c.1755delA/WT}$ mice injected with either AAV9-ctr or AAV9–PKP2. VIN is used as a loading control. **d**, Quantification of PKP2 protein levels. **e**, Quantification of MYC protein levels. **f**, Quantification of JUP protein levels. **g**, Quantification of DSP protein levels. **h**, Quantification of DSG2 protein levels. Experimental groups: *Pkp2*$^{WT/WT}$ mice injected with AAV9-ctr $n = 8$, *Pkp2*$^{WT/WT}$ mice injected with AAV9–PKP2 $n = 8$, *Pkp2*$^{c.1755delA/WT}$ mice injected with AAV9-ctr $n = 8$, *Pkp2*$^{c.1755delA/WT}$ mice injected with AAV9–PKP2 $n = 8$. **i**, Graph showing EF in *Pkp2*$^{WT/WT}$ and *Pkp2*$^{c.1755delA/WT}$ mice injected with either AAV9-ctr or AAV9-PKP2. **j**, Graph showing IVRT in *Pkp2*$^{WT/WT}$ and *Pkp2*$^{c.1755delA/WT}$ mice injected with either AAV9-ctr or AAV9-PKP2. **k**, Graph showing E/A ratio in *Pkp2*$^{WT/WT}$ and *Pkp2*$^{c.1755delA/WT}$ mice injected with either AAV9-ctr or AAV9–PKP2. These measurements correspond to 12-month-old mice. Data are presented as mean values ± s.e.m. Statistical significance is determined by one-way ANOVA (Tukey's post-hoc test), *P* value at $^{****}P < 0.0001$, $^{***}P < 0.001$, $^{**}P < 0.01$, $^{*}P < 0.05$, and not significant (NS). *P* value (*Pkp2*$^{c.1755delA/WT}$ + AAV9-ctr versus *Pkp2*$^{c.1755delA/WT}$ + AAV9-PKP2): 0.0101 (**d**), 0.0394 (**f**), 0.0052 (**g**), 0.0134 (**h**), 0.5622 (**i**), 0.0053 (**j**) and <0.0001 (**k**).

However, there is also evidence indicating that arrhythmias in ACM can manifest before structural abnormalities become apparent[42]. Notably, our 2D iPS-cell-derived CM cultures exhibited sodium conduction irregularities, indicating the presence of a proarrhythmic substrate in our models that may require additional triggers for arrhythmia manifestation (Fig. 2b,c).

So far cardiac gene therapy has been challenging due to a relatively low targeting efficiency owing to the complex architecture of the heart, being composed of multiple cell types. Despite the predominantly non-integrative nature of AAV vectors[43], multi-year transgene expression after gene transfer has been documented in large animals and humans[44–46]. The fact that we can detect the MYC epitope signal in murine CMs 10 months after the virus administration might be indicating that the promising 'one and done' AAV strategy employed in mice could potentially be feasible in human patients as well. In addition, our results indicate that PKP2 restoration in almost 70% of the CMs of the murine ventricles is sufficient to lead to a functional benefit in the mutant animals (Extended Data Fig. 6a,b). While AAV-based gene therapies have been shown to target the liver[29], our data indicated nonsignificant levels of exogenous PKP2 in the lung, spleen and kidneys of mice; however, moderate expression of cardiac PKP2 in the liver was observed (Extended Data Fig. 6d,e). Should it be desirable, liver targeting can be avoided by the use of a cardiac-specific promoter to drive *PKP2* expression, the use of a cardiotropic capsid and the addition of a liver detargeting sequence. For example, AAV2i8, AAV2i8G9 and AAV-SASTG chimeras, some AAV serotype 9 variants, or vectors obtained through the screening of peptide display libraries or DNA-shuffled libraries[47,48] all display improved cardio tropism. A cardiotropic capsid (BNP116) obtained as an AAV2/AAV8 chimera[49] is currently used in a gene therapy clinical trial for heart failure[50].

ACM is an inherited heart condition characterized by progressive structural changes in the myocardium, which increase the risk of arrhythmias and impair contractile function. In the absence of curative options, current therapeutic interventions for patients suffering from ACM are aimed at controlling disease progression and include antiarrhythmic medications, use of implantable cardioverter defibrillators, catheter ablation and often lifestyle changes[51]. Approaches that interfere with the underlying cause of the disease, in this case PKP2 haploinsufficiency, could potentially be more efficacious in halting or reversing the disease course. However, identification of the patient population that would benefit from *PKP2* gene therapy is currently challenging. Genetic testing could help to identify patients that could suffer from PKP2 haploinsufficiency[52]. However, this type of testing is usually reserved for individuals with a family history of cardiac disease or for those who have already been diagnosed with a cardiac condition and does not necessarily indicate what is happening at the protein level. Readouts in non-cardiac cells that express desmosomal proteins might provide a non-invasive tool to determine cardiac desmosomal protein content indirectly. Researchers have detected a significant reduction of JUP protein in buccal mucosa cells of patients with ACM compared to healthy counterparts[53,54]. Additionally, the PKP2 levels in keratinocytes has been shown to mirror the cardiac level of PKP2[13]. Such a non-invasive, quantitative method to assess cardiac levels of PKP2, combined with a comprehensive evaluation by a healthcare provider, could effectively identify patients that would benefit from *PKP2* gene replacement therapy.

So far, six AAV gene therapy products have already been approved for clinical use for non-cardiac indications, with over 1,400 patients having already been treated with onasemnogene[55], an intravenously administered AAV9 vector expressing the survival of motor neuron 1 (*SMN1*) protein for spinal muscular atrophy (SMA). After the initial drawback of the AAV1/*SERCA2α* gene therapy for heart failure, which failed in a large phase IIb clinical trial[56], gene therapy for the heart is also picking up speed again. AskBio takes advantage of a cardiotropic AAV vector with a chimeric AAV2/AAV8 capsid (BNP116)[49] to overexpress a constitutively active form of Inhibitor-1c (*I-1c*) in patients with heart failure (NCT04179643). Earlier this year, Rocket Pharmaceuticals has received regenerative medicine advanced therapy designation for an AAV9-based gene therapy to express the B isoform of the lysosomal associated membrane protein-2 (*LAMP-2*) to tackle Danon disease after the success of a phase I clinical trial (NCT03882437). On top of that, in May 2023 the same company received an Investigational New Drug (IND) approval for clinical gene therapy for *PKP2* for ACM patients, a highly promising development for the field's future. Tenaya Therapeutics has received fast track designation for a phase 1b clinical trial for *MYBPC3* gene replacement therapy for hypertrophic cardiomyopathy (NCT05836259), utilizing an optimized AAV9 vector to package the full-length *MYBPC3* gene. In addition, the company received orphan drug designation to its *PKP2* gene therapy product candidate TN-401 for treatment in 2022 with preclinical results in preparation and a filing for IND in 2023.

Overall, the potential of gene therapy in treating genetic diseases represents a paradigm shift in the way we approach these conditions. Although *PKP2* gene replacement therapy has demonstrated promise in preclinical studies using our knock-in mice, additional studies in suitable models are necessary to establish appropriate dosing regimens and determine potential safety issues. Heterogeneity in targeting of individual CMs could render the heart more susceptible to arrhythmias. A meticulous assessment of the risk of arrhythmias demands rigorous testing in larger animal models that accurately mimic human cardiac physiology in terms of heart rates, size, and function.

To conclude, our data support the notion that *PKP2* gene therapy holds promise for improving the clinical outcomes of patients with ACM with PKP2 haploinsufficiency, and reinforce the promise of gene therapy for tackling heart disease.

Methods

Human iPS cell lines

The human *PKP2* c.2013delC and *PKP2* c.1849C>T iPS cell lines were provided by H.-S. V. Chen at University of California San Diego[40] and J. Wu at Stanford Cardiovascular Institute (supported by National Institutes of Health R24 HL117756), respectively.

Cell culture

Human iPS cells were grown on Geltrex LDEV-Free, hESC-Qualified, Reduced Growth Factor Basement Membrane Matrix-coated wells (Gibco, A1413302). The cells received fresh Essential 8 Medium (Gibco, A1517001) on a daily basis and were passaged at 80–100% confluency levels. In brief, medium was aspirated and dissociation of the cells was performed with TrypLE Express Enzyme (Gibco, 12605010) for 5 min at 37 °C. After incubation, 4 ml of Essential 8 Medium, supplemented with 2 μM thiazovivin (Sigma-Aldrich, 420220), was added to the dissociated cells and transferred to a 15 ml Falcon tube. Cells were centrifuged for 3 min at 300*g*. Lastly, cells were seeded at a density of 15,000 cells cm^{-2} in Essential 8 Medium, supplemented with 2 μM thiazovivin. Medium was refreshed the next day with plain Essential 8.

CM differentiation

The differentiation protocol started when human iPS cells reached 80–90% of confluency (day 0). Cells were fed with RPMI-1640-Medium-GlutaMAX Supplement-HEPES (Gibco, 72400-021) supplemented with 0.5 mg ml^{-1} human recombinant albumin (Sigma-Aldrich, A9731), 0.2 mg ml^{-1} L-ascorbic acid 2-phosphate (Sigma-Aldrich, A8960) and 4 μM CHIR99021 (Sigma-Aldrich, 361559). After 48 h (day 2), medium was replaced by RPMI-1640-Medium-GlutaMAX Supplement-HEPES supplemented with 0.5 mg ml^{-1} human recombinant albumin (Sigma-Aldrich, A9731), 0.2 mg ml^{-1} L-ascorbic acid 2-phosphate and 5 μM IWP2 (Sigma-Aldrich, 681671). On day 4 and day 6, cells were refreshed with RPMI-1640-Medium-GlutaMAX Supplement-HEPES supplemented with 0.5 mg ml^{-1} human recombinant albumin and 0.2 mg ml^{-1} L-ascorbic acid 2-phosphate. From day 8 onwards, the medium of the cells was refreshed every 3–4 days with RPMI-1640-Medium-GlutaMAX Supplement-HEPES supplemented with B-27 Supplement (50×)-serum free (Gibco, 17504001).

CM purity

To assess the purity, 1×10^6 iiPS-cell-derived CMs at 15 days of age were utilized. The CMs were subjected to centrifugation at 300*g* for 5 min. The medium was removed, and cells were washed with Dulbecco's Phosphate-Buffered Saline (dPBS) (Gibco, 14190094). Following another centrifugation at 300*g* for 5 min, the dPBS was aspirated, and cells were fixed by adding 1 ml of ice-cold 70% ethanol while vortexing. After a subsequent centrifugation at 300*g* for 4 min, the fixative was removed. Permeabilization was achieved by resuspending the cells in blocking buffer consisting of PBS (pH 7.2–7.4), supplemented with 5% fetal bovine serum, 1% bovine serum albumin (Sigma-Aldrich, A9647-100G) and 0.5% Triton X-100 (Sigma-Aldrich, 93443). Following a 10-min incubation at 4 °C, permeabilized cells underwent another centrifugation for 4 min at 300*g*, and the supernatant was aspirated. The cell pellet was resuspended in 100 µl of blocking buffer containing anti-Cardiac Troponin T antibody (Abcam, ab45932; 1:2,000) and incubated at 4 °C for 1 h. Subsequently, 500 µl of blocking solution was added, and cells were centrifuged again for 4 min at 300*g*. After aspirating the supernatant, cells were resuspended once more in 500 µl of blocking buffer, followed by another centrifugation step for 4 min at 300*g*. Cells were then resuspended in 100 µl of blocking buffer containing Alexa 488-anti-rabbit antibody (Thermo Fisher Scientific, A-21206; 1:4,000) and incubated for 30 min at room temperature. Next, 500 µl of blocking buffer was added, and cells were centrifuged for 4 min at 300*g*. The supernatant was discarded, and cells were resuspended again with 500 µl of blocking buffer, followed by another centrifugation for 4 min at 300*g*. Finally, the supernatant was aspirated, and cells were resuspended in 1 ml of dPBS for analysis by fluorescence-activated cell sorting (BD Biosciences, FACS Calibur).

Automated patch clamp

iPS-cell-derived CM collection proceeded with a PBS wash followed by a Versene wash before dissociation with TrypLE Express (all: Gibco) for 10 min at 37 °C. The cells were resuspended in divalent-free HBSS (Gibco) at 4 °C before measurement. Automated patch clamp experiments were conducted with the SyncroPatch 384 (Nanion Technologies GmbH) device with thin borosilicate glass, single aperture 384-well chips (NPC384T 1× S-type). Application of negative pressure (150–250 mbar) attained whole-cell configuration. I_{Na} recordings were performed at 0.5 Hz using a voltage step protocol with a holding potential of −80 mV followed by a hyperpolarizing step to −110 mV for 100 ms and a 300-ms test pulse to −20 mV. Pipette solution contained (in mmol l^{-1}): egtazic acid 10, HEPES 10, KCl 10, NaCl 10 and KF 110, pH 7.2 (with KOH). Bath solution contained (in mmol l^{-1}): HEPES 10, NaCl 80, N-methyl-d-glucamine (NMDG) 60, glucose 5, KCl 4, $CaCl_2$ 2 and $MgCl_2$ 1, pH 7.4 at 22–24 °C (with KOH). Currents were recorded with an integrated amplifier controlled by PatchControl 384 software and analyzed offline using DataControl 384 software (both: Nanion Technologies GmbH)[57].

EHM generation

EHM was generated according to the protocol published by Tiburcy et al.[58]. In brief, patient-derived iPS-cell-derived CMs (purity >90%) were mixed together with HFFs (HFF-1, ATCC, SCRC-1041) at a ratio of 70:30. The cell mixture was resuspended in an appropriate volume of Collagen type I (Collagen Solutions, FS22024) diluted into RPMI 2× (Thermo Fisher Scientific, 51800-035). A total of 185 µl of the cell–collagen mixture was cast in each well of a 48 EHM multi-well plate (myrPlate-TM5; myriamed GmbH). The cast mixture was incubated for approximately 45 min at 37 °C and subsequently EHM medium freshly supplemented with TGFβ1 (Peprotech, AF-100-21C) was added. During the initial 3 days following the casting process, tissue medium was refreshed daily with EHM medium supplemented with TGFβ1. Subsequently, the tissue medium was replaced daily with EHM medium for the entirety of the experimental duration.

Contraction analyses

Contraction measurements were performed using video-optic recordings of EHM mediated pole bending in a myrPlate-TM5 culture format at 37 °C (ref. 59). Data were recorded from spontaneously contraction EHM for at least 2 min at 50 fps at the indicated time points in a myrImager prototype (myriamed GmbH). Percent pole bending is reported as a surrogate for force of contraction (*F*); contraction and relaxation times are recorded from 20% to 80% peak contraction and 20% to 80% relaxation; contraction and relaxation velocities are reported as maximal and mininmal d*F*/d*t*.

Quantitative real-time PCR

For iPS-cell-derived CMs, RNA isolation was performed utilizing the RNeasy kit (Qiagen, 74104) as per the manufacturer's guidelines. Complementary DNA synthesis was conducted using the iScript cDNA Synthesis Kit (Bio-Rad). Quantitative PCR analysis was carried out using the CFX96 Realtime PCR system (Bio-Rad) and iQ SYBR Green (Bio-Rad) in accordance with the manufacturers' instructions (Supplementary Table 1).

Mouse line generation

All animal studies carried out in this research adhered to the institutional guidelines and complied with the regulations set forth by the Animal Welfare Committee of the Royal Netherlands Academy of Arts and Sciences. Animal experiments were conducted upon approval by the 'Animal Welfare Body Utrecht' (I.v.D.) of the Royal Dutch Academy of Sciences and Arts (K.N.A.W.) and are in compliance with national legislation and institutional guidelines.

Mouse lines were maintained on C57B/6J background. Male and female mice were included in studies performed in pups, whereas studies in adult mice only included males.

Echocardiographic analysis

Isoflurane-anesthetized mice were subjected to transthoracic M-mode echocardiographic recordings while placed on a heat mat. The recordings were conducted using a Visual Sonic Ultrasound System connected to a 30 MHz transducer. For each mouse, three measurements were taken for various cardiac parameters including LVEDV, LVESV, end-diastolic interventricular septal wall thickness, end-systolic interventricular septal wall thickness, IVRT and the early (E) and late (A) ventricular filling velocities. The E and A values were utilized to calculate the E/A ratio. Cardiac function, specifically EF (%), was automatically determined by the software using the averaged values of the aforementioned parameters.

Histology and immunohistochemistry

Cardiac tissue from mice or EHM was collected and briefly washed in ice-cold PBS. After rinsing and weighing, they were fixed in 4% paraformaldehyde for 48 or 24 h, respectively, at room temperature. The fixed tissues were then embedded in paraffin and sliced at 4 µm. The sections were dewaxed and rehydrated. For immunohistochemistry, tissue sections were boiled for 20 min in either ethylenediaminetetraacetic acid (EDTA) buffer or sodium citrate buffer. They were then blocked for 45 min at room temperature using a solution containing 0.1% bovine serum albumin and 0.4% TWEEN20 dissolved in dPBS. The tissue was then incubated with primary antibodies overnight at 4 °C, followed by incubation with secondary antibodies for 1 h at room temperature. DAPI diluted in dPBS (1:1,000) was used to stain the sections, and they were subsequently mounted with Mowiol and imaged using a Leica TCS SPE confocal microscope. Leica Application Suite (LAS X, version 3.30 or newer) was used for image acquisition, whereas image processing was performed with Fiji. Supplementary Table 2 presents information about all antibodies used for immunofluorescence assays.

Western blot

iPS-cell-derived CMs were dissociated using TrypLE Select Enzyme (10×) and collected in a 1.5-ml Eppendorf tube. The cells were then centrifuged at 300*g* for 5 min and resuspended in 1 ml of dPBS, followed by another centrifugation round with the same conditions. The cells were then lysed in RIPA buffer containing cOmplete EDTA-free Protease Inhibitor Cocktail (one tablet per 10 ml of RIPA buffer) and PhosSTOP (one tablet per 10 ml of RIPA buffer). For immunoblotting, 10–15 µg of protein extract was used. Horseradish peroxidase-coupled secondary antibodies were used in combination with the Clarity Western ECL Substrate kit for visualization. Immunoblots were imaged using an Amersham Imager 680RGB device and quantified with ImageQuant TL software v7.1 (GE Healthcare).

Immunoblotting was also performed on protein lysates from snap-frozen mouse tissue explanted from the ventricles. The tissue was lysed in approximately 150 µl of RIPA buffer as described above. Immunoblotting was performed using 20–50 µg of protein. In Supplementary Table 3 there are all details regarding antibodies used.

AAV delivery

AAV vectors (serotype 6 or 9) encoding human *PKP2*, murine *Pkp2* or empty vector were generated in collaboration with the Giacca and Zentilin labs (Trieste, Italy).

We used 5×10^3 v.g. per cell to infect hiPS-cell-derived CMs with AAV6. AAV9-ctr and AAV9–PKP2 were used for in vivo studies. A total of 3×10^{11} v.g. per animal were injected intraperitoneally into 5-day-old pups using an insulin syringe with a 30-gauge needle. Adult mice were injected intravenously through the tail vein with 5×10^{12} v.g. per animal (one single injection) using a syringe with a 26-gauge needle.

Statistical analysis

Data are presented as mean ± standard error of the mean. Statistical differences between two groups were tested by two-sided unpaired or paired Student's *t*-tests. In case of three and more groups, one-way or two-way unrepeated or repeated-measures analysis of variance (ANOVA) with appropriate post-hoc testing was performed. The performed tests are specified in the respective figure legends. Statistical testing was performed with GraphPad Prism 9.5.1.

Reporting summary

Further information on research design is available in the Nature Portfolio Reporting Summary linked to this article.

Data availability

All data supporting the findings in this study are available within the paper and associated files. Source data are provided with this paper.

References

1. Pilichou, K. et al. Arrhythmogenic cardiomyopathy. *Orphanet J. Rare Dis.* **11**, 33 (2016).
2. Sen-Chowdhry, S. et al. Mutational heterogeneity, modifier genes, and environmental influences contribute to phenotypic diversity of arrhythmogenic cardiomyopathy. *Circ. Cardiovasc. Genet.* **3**, 323–330 (2010).
3. Basso, C., Corrado, D., Bauce, B. & Thiene, G. Arrhythmogenic right ventricular cardiomyopathy. *Circ. Arrhythm. Electrophysiol.* **5**, 1233–1246 (2012).
4. Giuliano, K. et al. Heart transplantation outcomes in arrhythmogenic right ventricular cardiomyopathy: a contemporary national analysis. *ESC Heart Fail.* **9**, 988–997 (2022).
5. Marcus, F. I. et al. Diagnosis of arrhythmogenic right ventricular cardiomyopathy/dysplasia: proposed modification of the Task Force Criteria. *Eur. Heart J.* **31**, 806–814 (2010).
6. Vermij, S. H., Abriel, H. & van Veen, T. A. Refining the molecular organization of the cardiac intercalated disc. *Cardiovasc. Res.* **113**, 259–275 (2017).
7. van Hengel, J. et al. Mutations in the area composita protein αT-catenin are associated with arrhythmogenic right ventricular cardiomyopathy. *Eur. Heart J.* **34**, 201–210 (2013).
8. Agullo-Pascual, E., Cerrone, M. & Delmar, M. Arrhythmogenic cardiomyopathy and Brugada syndrome: diseases of the connexome. *FEBS Lett.* **588**, 1322–1330 (2014).
9. Sato, P. Y. et al. Interactions between ankyrin-G, Plakophilin-2, and Connexin43 at the cardiac intercalated disc. *Circ. Res.* **109**, 193–201 (2011).
10. Jacob, K. A. et al. Geographical distribution of plakophilin-2 mutation prevalence in patients with arrhythmogenic cardiomyopathy. *Neth. Heart J.* **20**, 234–239 (2012).
11. Basharat, S. A., Hsiung, I., Garg, J. & Alsaid, A. Arrhythmogenic cardiomyopathy: evolving diagnostic criteria and insight from cardiac magnetic resonance imaging. *Heart Fail. Clin.* **19**, 429–444 (2023).
12. Hylind, R. J. et al. Population prevalence of premature truncating variants in plakophilin-2 and association with arrhythmogenic right ventricular cardiomyopathy: a UK Biobank analysis. *Circ. Genom. Precis. Med.* **15**, e003507 (2022).
13. Rasmussen, T. B. et al. Truncating plakophilin-2 mutations in arrhythmogenic cardiomyopathy are associated with protein haploinsufficiency in both myocardium and epidermis. *Circ. Cardiovasc. Genet.* **7**, 230–240 (2014).
14. Zhang, K. et al. Plakophilin-2 truncating variants impair cardiac contractility by disrupting sarcomere stability and organization. *Sci. Adv.* **7**, eabh3995 (2021).
15. Cerrone, M. et al. Plakophilin-2 is required for transcription of genes that control calcium cycling and cardiac rhythm. *Nat. Commun.* **8**, 106 (2017).
16. Goossens, S. et al. A unique and specific interaction between αT-catenin and plakophilin-2 in the area composita, the mixed-type junctional structure of cardiac intercalated discs. *J. Cell Sci.* **120**, 2126–2136 (2007).
17. Pérez-Hernández, M. et al. Transcriptomic coupling of PKP2 with inflammatory and immune pathways endogenous to adult cardiac myocytes. *Front. Physiol.* **11**, 623190 (2020).
18. Dubash, A. D. et al. Plakophilin-2 loss promotes TGF-β1/p38 MAPK-dependent fibrotic gene expression in cardiomyocytes. *J. Cell Biol.* **212**, 425–438 (2016).
19. Liang, Y. et al. Desmosomal COP9 regulates proteome degradation in arrhythmogenic right ventricular dysplasia/cardiomyopathy. *J. Clin. Invest.* **131**, e137689 (2021).
20. Tsui, H. et al. Desmosomal protein degradation as an underlying cause of arrhythmogenic cardiomyopathy. *Sci. Transl. Med.* **15**, eadd4248 (2023).
21. Pérez-Hernández, M. et al. Loss of nuclear envelope integrity and increased oxidant production cause DNA damage in adult hearts deficient in PKP2: a molecular substrate of ARVC. *Circulation* **146**, 851–867 (2022).
22. van Opbergen, C. J. M. et al. Plakophilin-2 haploinsufficiency causes calcium handling deficits and modulates the cardiac response towards stress. *Int. J. Mol. Sci.* **20**, 4076 (2019).
23. Peters, S. Editorial: cardiomyopathies: current treatment and future options. *J. Clin. Med.* **9**, 3531 (2020).
24. Bosman, L. P. et al. The Netherlands Arrhythmogenic Cardiomyopathy Registry: design and status update. *Neth. Heart J.* **27**, 480–486 (2019).
25. Groeneweg, J. A. et al. Clinical presentation, long-term follow-up, and outcomes of 1001 arrhythmogenic right ventricular dysplasia/cardiomyopathy patients and family members. *Circ. Cardiovasc. Genet.* **8**, 437–446 (2015).

26. Cerrone, M. et al. Sodium current deficit and arrhythmogenesis in a murine model of plakophilin-2 haploinsufficiency. *Cardiovasc. Res.* **95**, 460–468 (2012).
27. Shaw, R. M. Reduced sodium channels in human ARVC. *Heart Rhythm* **10**, 420–421 (2013).
28. Tiburcy, M., Meyer, T., Satin, P. L. & Zimmermann, W. H. Defined engineered human myocardium for disease modeling, drug screening, and heart repair. *Methods Mol. Biol.* **2485**, 213–225 (2022).
29. Zincarelli, C., Soltys, S., Rengo, G. & Rabinowitz, J. E. Analysis of AAV serotypes 1–9 mediated gene expression and tropism in mice after systemic injection. *Mol. Ther.* **16**, 1073–1080 (2008).
30. Inoue, H. et al. Modeling reduced contractility and impaired desmosome assembly due to plakophilin-2 deficiency using isogenic iPS cell-derived cardiomyocytes. *Stem Cell Rep.* **17**, 337–351 (2022).
31. Tardiff, J. C. et al. Targets for therapy in sarcomeric cardiomyopathies. *Cardiovasc. Res.* **105**, 457–470 (2015).
32. Prondzynski, M. et al. Evaluation of MYBPC3 *trans*-splicing and gene replacement as therapeutic options in human iPSC-derived cardiomyocytes. *Mol. Ther. Nucleic Acids* **7**, 475–486 (2017).
33. Mearini, G. et al. Mybpc3 gene therapy for neonatal cardiomyopathy enables long-term disease prevention in mice. *Nat. Commun.* **5**, 5515 (2014).
34. Palatinus, J. A. et al. GJA1-20k rescues Cx43 localization and arrhythmias in arrhythmogenic cardiomyopathy. *Circ. Res.* **132**, 744–746 (2023).
35. Clauss, S. et al. Animal models of arrhythmia: classic electrophysiology to genetically modified large animals. *Nat. Rev. Cardiol.* **16**, 457–475 (2019).
36. Gussak, I., Chaitman, B. R., Kopecky, S. L. & Nerbonne, J. M. Rapid ventricular repolarization in rodents: electrocardiographic manifestations, molecular mechanisms, and clinical insights. *J. Electrocardiol.* **33**, 159–170 (2000).
37. Liu, G. et al. In vivo temporal and spatial distribution of depolarization and repolarization and the illusive murine T wave. *J. Physiol.* **555**, 267–279 (2004).
38. Sommariva, E. et al. Cardiac mesenchymal stromal cells are a source of adipocytes in arrhythmogenic cardiomyopathy. *Eur. Heart J.* **37**, 1835–1846 (2016).
39. Caspi, O. et al. Modeling of arrhythmogenic right ventricular cardiomyopathy with human induced pluripotent stem cells. *Circ. Cardiovasc. Genet.* **6**, 557–568 (2013).
40. Kim, C. et al. Studying arrhythmogenic right ventricular dysplasia with patient-specific iPSCs. *Nature* **494**, 105–110 (2013).
41. Asimaki, A., Kleber, A. G. & Saffitz, J. E. Pathogenesis of arrhythmogenic cardiomyopathy. *Can. J. Cardiol.* **31**, 1313–1324 (2015).
42. Gomes, J. et al. Electrophysiological abnormalities precede overt structural changes in arrhythmogenic right ventricular cardiomyopathy due to mutations in desmoplakin-A combined murine and human study. *Eur. Heart J.* **33**, 1942–1953 (2012).
43. Li, H. et al. Assessing the potential for AAV vector genotoxicity in a murine model. *Blood* **117**, 3311–3319 (2011).
44. Nathwani, A. C. et al. Long-term safety and efficacy following systemic administration of a self-complementary AAV vector encoding human FIX pseudotyped with serotype 5 and 8 capsid proteins. *Mol. Ther.* **19**, 876–885 (2011).
45. Nathwani, A. C. et al. Long-term safety and efficacy of factor IX gene therapy in hemophilia B. *N. Engl. J. Med.* **371**, 1994–2004 (2014).
46. Niemeyer, G. P. et al. Long-term correction of inhibitor-prone hemophilia B dogs treated with liver-directed AAV2-mediated factor IX gene therapy. *Blood* **113**, 797–806 (2009).
47. Zacchigna, S., Zentilin, L. & Giacca, M. Adeno-associated virus vectors as therapeutic and investigational tools in the cardiovascular system. *Circ. Res.* **114**, 1827–1846 (2014).
48. Grimm, D. & Büning, H. Small but increasingly mighty: latest advances in AAV vector research, design, and evolution. *Hum. Gene Ther.* **28**, 1075–1086 (2017).
49. Ishikawa, K. et al. Cardiac I-1c overexpression with reengineered AAV improves cardiac function in swine ischemic heart failure. *Mol. Ther.* **22**, 2038–2045 (2014).
50. NAN-101 in patients with class III heart failure (NAN-CS101). *National Library of Medicine* https://clinicaltrials.gov/ct2/show/NCT04179643. (2019).
51. Migliore, F. et al. Arrhythmogenic cardiomyopathy—current treatment and future options. *J. Clin. Med.* **10**, 2750 (2021).
52. de Brouwer, R. et al. Value of genetic testing in the diagnosis and risk stratification of arrhythmogenic right ventricular cardiomyopathy. *Heart Rhythm* **19**, 1659–1665 (2022).
53. Asimaki, A. et al. Characterizing the molecular pathology of arrhythmogenic cardiomyopathy in patient buccal mucosa cells. *Circ. Arrhythm. Electrophysiol.* **9**, e003688 (2016).
54. Driessen, H. E. et al. Buccal mucosa cells as a potential diagnostic tool to study onset and progression of arrhythmogenic cardiomyopathy. *Int. J. Mol. Sci.* **23**, 57 (2021).
55. Aslesh, T. & Yokota, T. Restoring SMN expression: an overview of the therapeutic developments for the treatment of spinal muscular atrophy. *Cells* **11**, 417 (2022).
56. Greenberg, B. et al. Calcium upregulation by percutaneous administration of gene therapy in patients with cardiac disease (CUPID 2): a randomised, multinational, double-blind, placebo-controlled, phase 2b trial. *Lancet* **387**, 1178–1186 (2016).
57. Seibertz, F. et al. A modern automated patch-clamp approach for high throughput electrophysiology recordings in native cardiomyocytes. *Commun. Biol.* **5**, 969 (2022).
58. Tiburcy, M. et al. Defined engineered human myocardium with advanced maturation for applications in heart failure modeling and repair. *Circulation* **135**, 1832–1847 (2017).
59. Tiburcy, M., Meyer, T., Liaw, N. Y. & Zimmermann, W. H. Generation of engineered human myocardium in a multi-well format. *STAR Protoc.* **1**, 100032 (2020).

Acknowledgements

This study was funded by: Dutch CardioVascular Alliance with support of the Dutch Heart Foundation, DCVA2017-18 ARENA-PRIME (E.v.R). Dutch CardioVascular Alliance with support of the Dutch. Heart Foundation, DCVA2015-12 eDETECT (J.P.v.T.). Dutch CardioVascular Alliance. with support of the Dutch Heart Foundation, DCVA2018-30 PREDICT2 (J.P.v.T.). Vici grant from the Dutch Research Council (NWO), project 09150181910020 (E.v.R). European Research Council (ERC) Advanced Grant 787971 'CuRE' (M.G.); British Heart Foundation (BHF) Programme Grant RG/19/11/34633 (M.G.); grants 825670 'CardioReGenix' and 874764 'REANIMA' from the European Commission Horizon 2020 programme (M.G.). German Research Foundation (DFG, VO 1568/3-1, VO 1568/4-1, SFB1002 A13, C04, S01, under Germany's Excellence Strategy—EXC 2067/1-390729940 to N.V., M.T. and W.H.Z.), by the DZHK (German Center for Cardiovascular Research, N.V., M.T. and W.H.Z, 81 × 4300102, 'DNAfix' to N.V.), the German Federal Ministry of Education and Research (IndiHEART; 161L0250A; T.M. and W.H.Z.), and the Fondation Leducq (20CVD04) (E.v.R., M.G. and W.H.Z). We would like to acknowledge the Netherlands ACM/PLN Registry, a nationwide observational cohort study, involving individuals diagnosed with ACM and their relatives who are at risk of the condition. This registry is managed by the Netherlands Heart Institute (NHI) located in Utrecht, the Netherlands. The study strictly adheres to the guidelines outlined in the Code of Conduct and Data Usage in Health Research. We gratefully

acknowledge Branimir Berecic and Daria Reher for for their invaluable contributions and dedication in training us on EHM construction and providing support in cell culture, respectively.

Author contributions

Conceptualization: E.v.R. and E.K. Data collection: E.K., D.V., H.R., I.P., F.S. and Y.D. Resources: H.T., S.J.v.K., L.Z. and J.P.v.T. Data analysis: E.K., H.R. and F.S. Funding acquisition: M.T., N.V., W.H.Z., M.G. and E.v.R. Software development: T.M. Writing—original draft: E.K. and E.v.R. Writing—review and editing: all authors

Competing interests

E.v.R. is a consultant for Tenaya Therapeutics and Novo Nordisk and is Chief Scientific Officer of Phlox Therapeutics. M.T., T.M. and W.H.Z. are inventors of patents related to the EHM technology and scientific advisors to myriamed GmbH. W.H.Z. is founder and shareholder of myriamed GmbH. M.G. is founder, consultant, member of the Board and equity holder in Purespring Therapeutics, Forcefield Therapeutics and Heqet Therapeutics. All other authors declare that they have no competing interests.

Additional information

Extended data is available for this paper at https://doi.org/10.1038/s44161-023-00378-9.

Supplementary information The online version contains supplementary material available at https://doi.org/10.1038/s44161-023-00378-9.

Correspondence and requests for materials should be addressed to Eva van Rooij.

Peer review information *Nature Cardiovascular Research* thanks Professor Silvia Priori, and the other, anonymous, reviewer(s) for their contribution to the peer review of this work.

https://doi.org/10.1038/s44161-023-00378-9

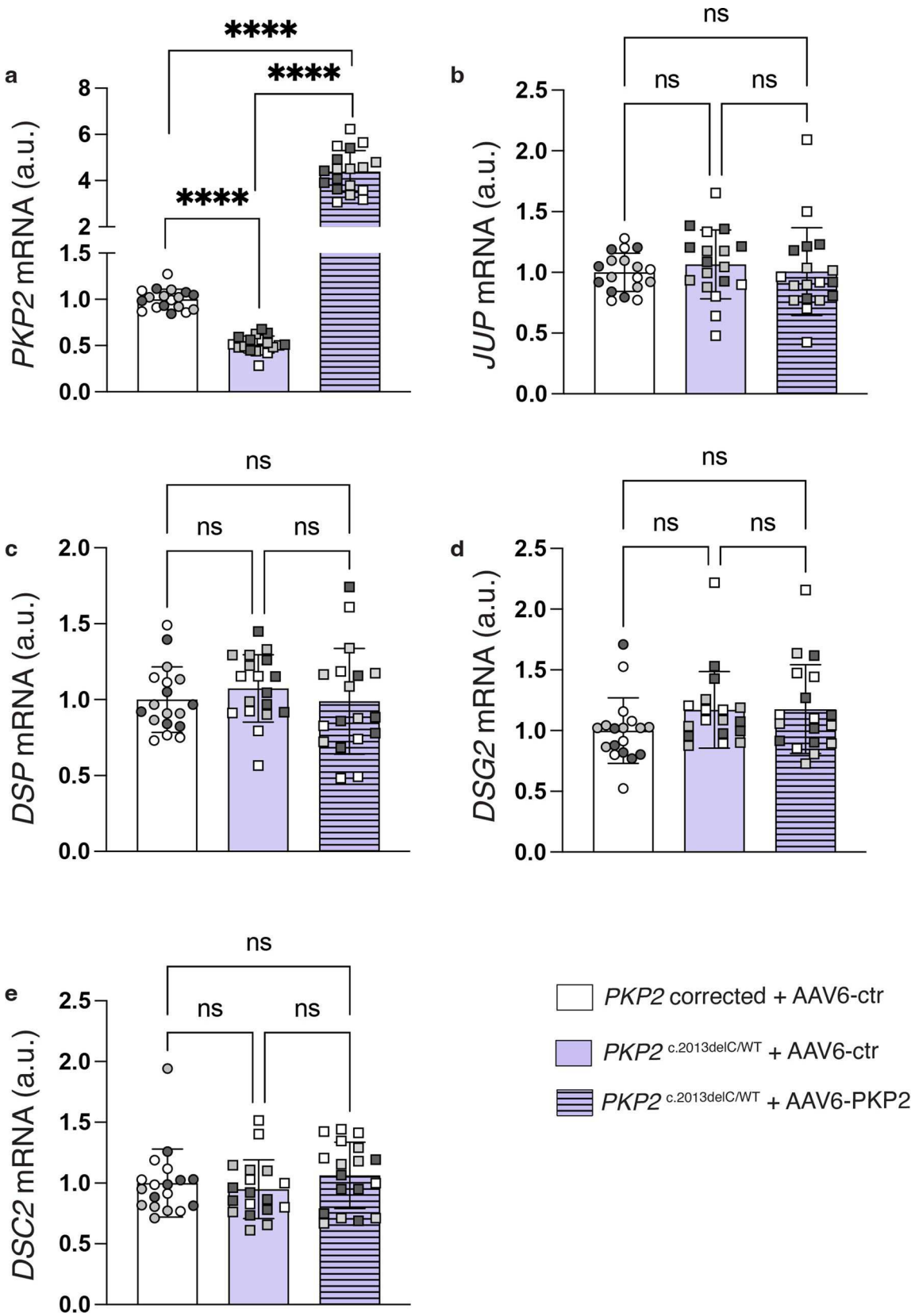

Extended Data Fig. 1 | AAV-mediated restoration of PKP2 in *PKP2*$^{c.2013delC/WT}$ mutant iPS-cell-derived CMs does not affect the mRNA levels of desmosomal proteins. a-e, Gene expression of *PKP2*, *JUP*, *DSP*, *DSG2* and *DSC2* in *Pkp2*$^{c.2013delC/WT}$ iPS-cell-derived CMs upon transduction with either AAV6-ctr or AAV6-PKP2. As a reference, the *PKP2* corrected iPS-cell-derived CM line was transduced with AAV6-ctr. Values were normalized to *GUS*. n = 3 biological replicates (distinct CM differentiations) and 6 technical replicates per differentiation. Data is presented as mean +/− s.e.m. Statistical significance is derived from biological replicates and is determined with one-way ANOVA (Tukey's post-hoc test), p-value at ****$P < 0.0001$, ***$P < 0.001$, **$P < 0.01$, *$P < 0.05$, and not significant (ns). Exact P-value for panel (a) is < 0.0001 for all comparisons.

https://doi.org/10.1038/s44161-023-00378-9

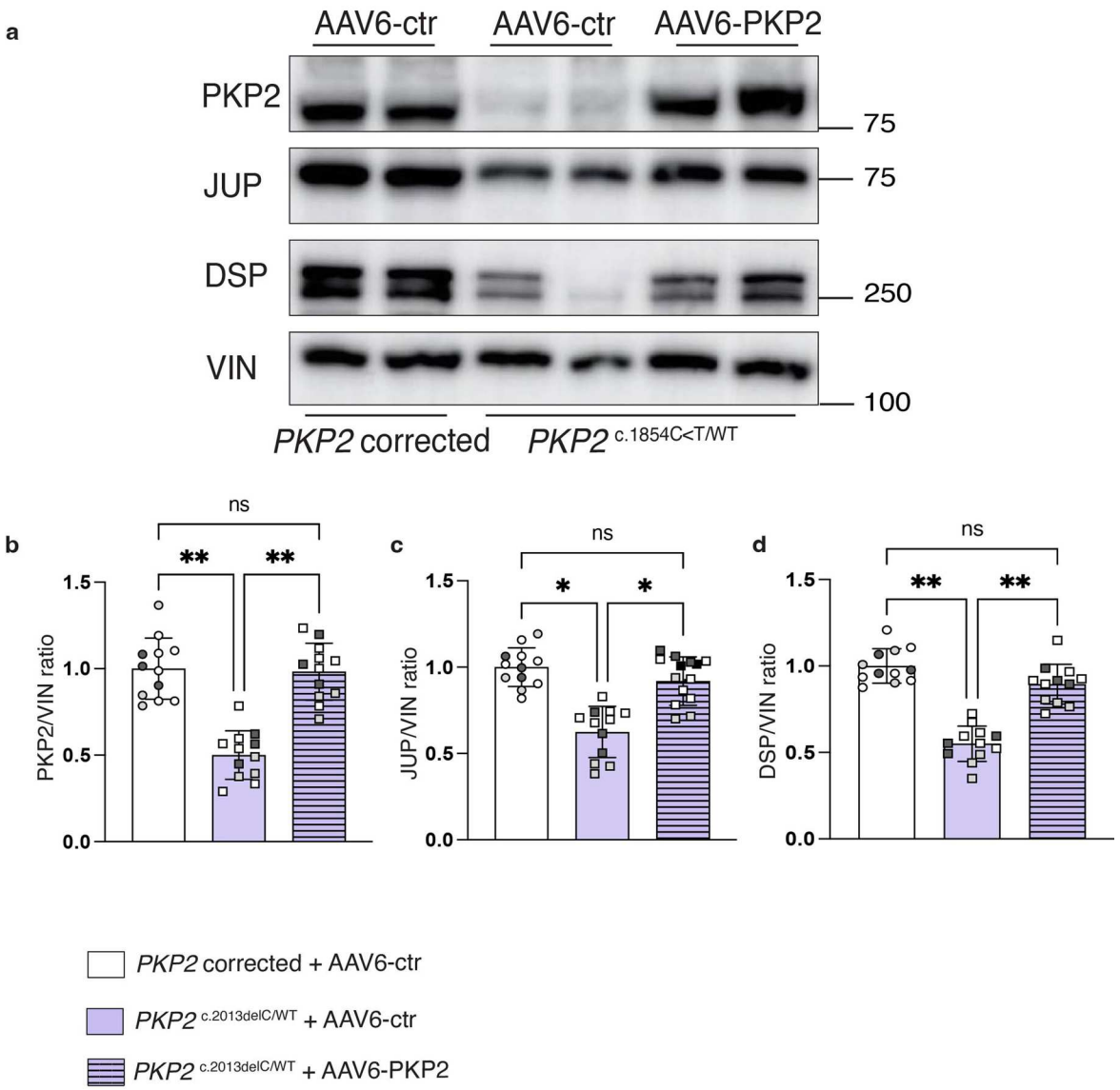

Extended Data Fig. 2 | PKP2 restoration in iPS-cell-derived CMs harboring the pathogenic variant *PKP2* c.1845C < T, leads to a recovery of JUP and DSP protein levels. a, Representative immunoblots for PKP2, JUP and DSP in *PKP2*$^{c.1845C<T/WT}$ iPS-cell CMs upon transduction with AAV6-ctr or AAV6-PKP2. VIN was used as a loading control. **b-d**, Quantification of (a), n = 3 biological replicates (distinct differentiations) and 6, 3 and 3 technical replicates per differentiation respectively. Data is presented as mean +/− s.e.m. Statistical significance is derived from biological replicates and is determined with one-way ANOVA (Tukey's post-hoc test) with p-value at $^{****}P < 0.0001$, $^{***}P < 0.001$, $^{**}P < 0.01$, $^{*}P < 0.05$, and not significant (ns). *P*-values (*PKP2*$^{c.1845C<T/WT}$+ AAV6-ctr vs *PKP2*$^{c.1845C<T/WT}$+ AAV6-PKP2): (b) = 0.016, (c) = 0.0366, (d) = 0.0016.

https://doi.org/10.1038/s44161-023-00378-9

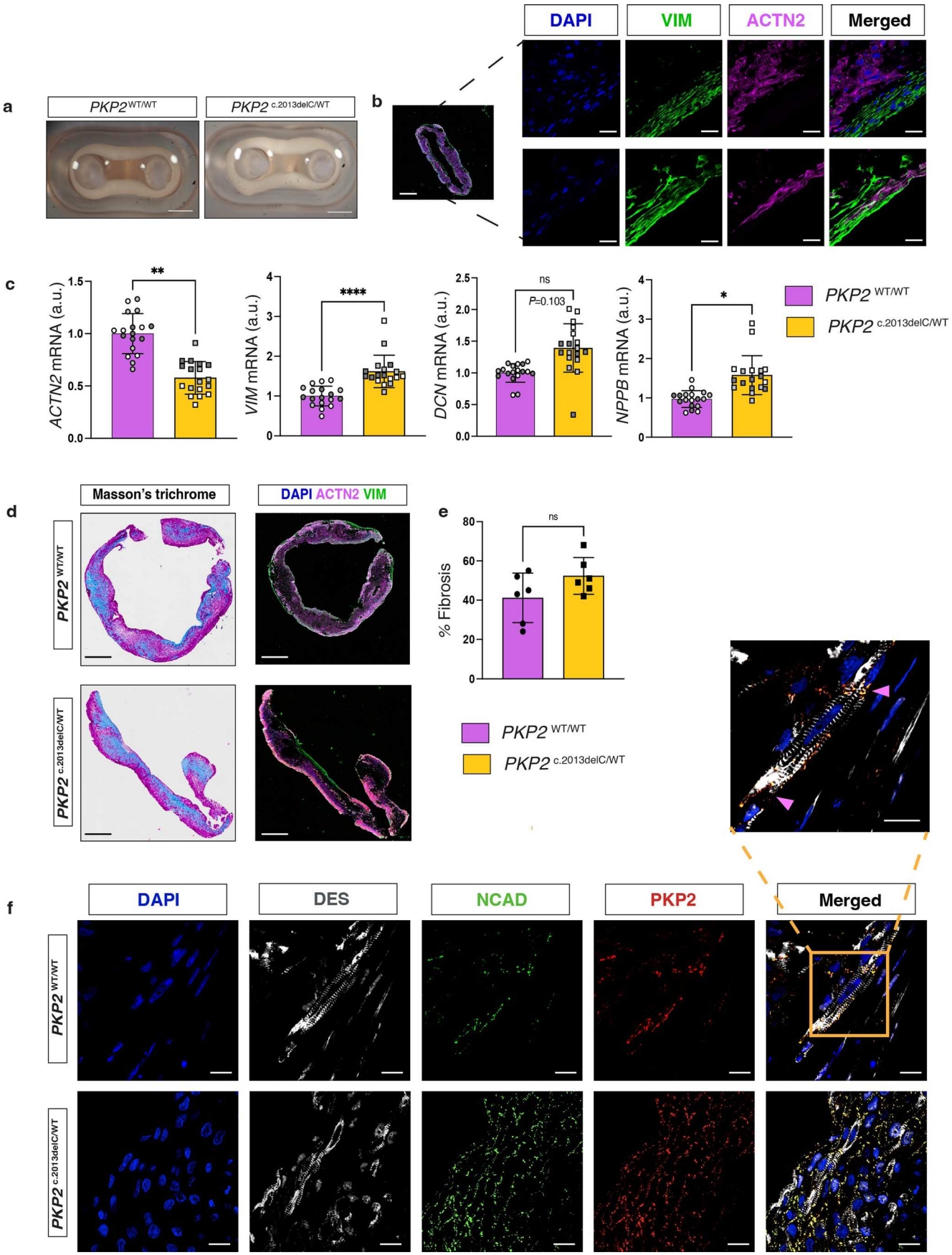

Extended Data Fig. 3 | See next page for caption.

https://doi.org/10.1038/s44161-023-00378-9

Extended Data Fig. 3 | The *PKP2* mutant EHM exhibit similar structural and intercellular junction organization as its isogenic control. a, Representative brightfield images of 6-week-old mutant and isogenic control EHM under baseline. Scale bar is at 1mm. **b**, On the left side: representative overview immunofluorescent staining of a paraffin-embedded EHM section. Scale bar is at 500µm. On the right side: representative high magnification fluorescent images of the same EHM section to show cardiomyocyte and fibroblast regions within the tissue. DAPI = blue, VIM = magenta, ACTN2 = green. Scale bar is at 20µm. **c**, Gene expression of ACTN2, VIM, DCN and NPPB on the mutant tissues compared to the isogenic control. Data is normalized to the housekeeping gene *GUS*. Colored dots represent distinct CM differentiations, n = 6 technical replicates and 3 biological replicates per condition. Data is presented as means +/− s.e.m. Statistical significance is derived from biological replicates and is determined by unpaired, two-tailed Student t-test, p-value at *****$P < 0.0001$, ***$P < 0.001$, **$P < 0.01$, *$P < 0.05$, and not significant (ns). ACTN2: P-value = 0.0077, VIM: P-value < 0.0001, DCN: P-value = 0.1033, NPPB: P-value = 0.0401. **d**, *On the left column:* representative images of a Masson's trichrome staining on paraffin-embedded EHM. Collagen = blue, muscle = red and nuclei = brown. *On the right column:* representative immunofluorescent images from paraffin-embedded EHM. ACTN2 = magenta, VIM = green and DAPI = in blue. Scale bar is at 500 µm. **e**, Quantification of the Masson's trichrome staining in (d). Each dot represents a mouse. Data is presented as means +/− s.e.m. Statistical significance is determined by unpaired, two-tailed Student t-test, p-value at ****$P < 0.0001$, ***$P < 0.001$, **$P < 0.01$, *$P < 0.05$, and not significant (ns). **f**, Representative immunofluorescent images displaying the intercalated disc (ID) structure on EHM. NCAD = green, PKP2 = red, DES = gray and DAPI = blue. Scale bar is at 20µm and at 10µm for the zoomed image on the top right. Pink arrowheads indicate a representative ID-like structure on a cardiomyocyte. This experiment has been performed three times independently with similar results.

https://doi.org/10.1038/s44161-023-00378-9

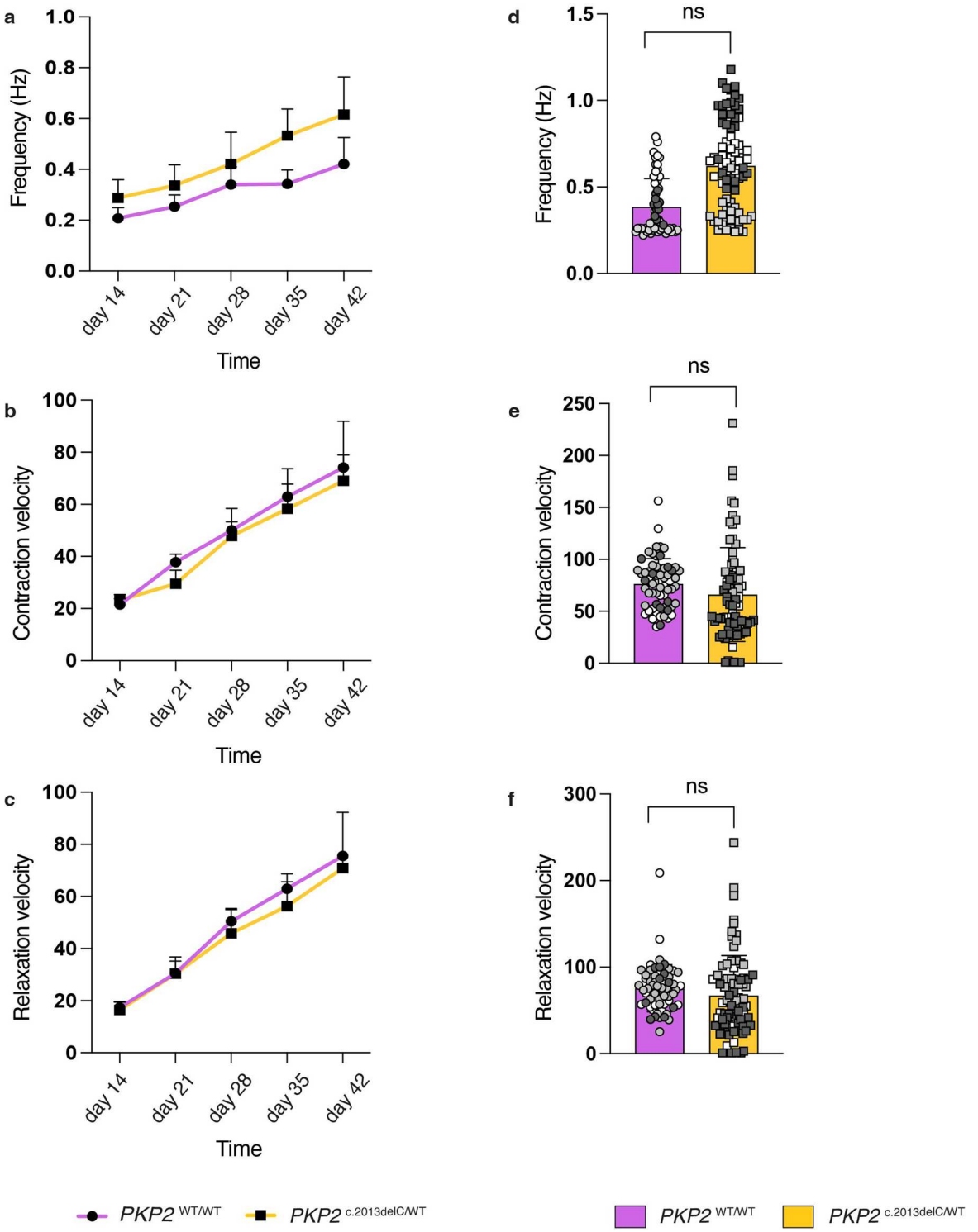

Extended Data Fig. 4 | *PKP2*$^{c.2013delC/WT}$ EHM do not exhibit an altered beating frequency, contraction velocity and relaxation velocity compared to control. a-c, Trendlines showing beating frequency (Hz), contraction velocity and relaxation velocity in *PKP2*$^{WT/WT}$ and *PKP2*$^{c.2013delC/WT}$ EHM at different timepoints after transduction with either AAV6-PKP2 or AAV6-ct, n = 3 biological replicates (three distinct EHM batches). **d-f**, Graphs displaying beating frequency (Hz), contraction velocity and relaxation velocity in *PKP2*$^{WT/WT}$ and *PKP2*$^{c.2013delC/WT}$ EHM after transduction with either AAV6-PKP2 or AAV6-ctr, on day 42 of maturation, n = 3 biological replicates (three distinct EHM batches), batch 1 = 17 isogenic control and 19 mutant tissues, batch 2 = 32 isogenic control and 27 mutant tissues and batch 3 = 11 isogenic control and 30 mutant tissues. Data is presented as means +/− s.e.m. Statistical significance is derived by biological replicates and is determined by unpaired, two-tailed Student t-test p-value at $^{****}P < 0.0001$, $^{***}P < 0.001$, $^{**}P < 0.01$, $^{*}P < 0.05$, and not significant (ns).

https://doi.org/10.1038/s44161-023-00378-9

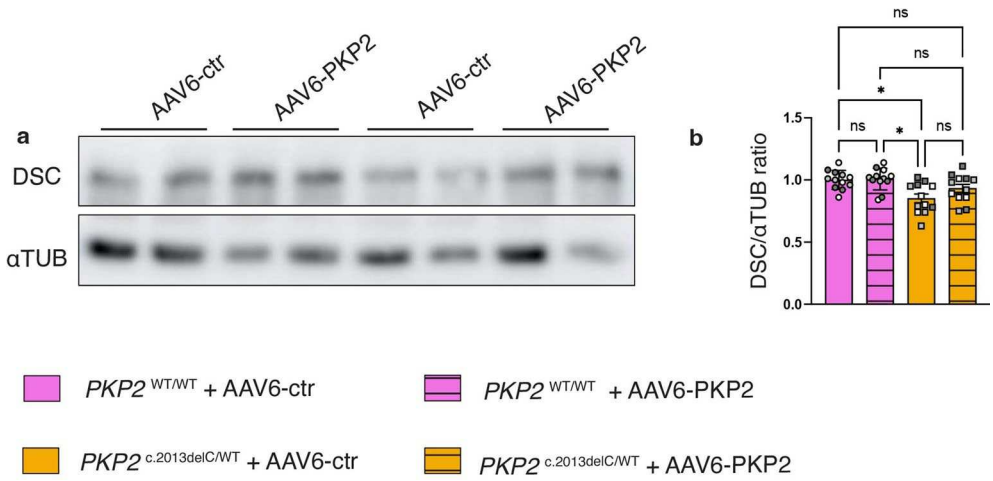

Extended Data Fig. 5 | AAV-PKP2 treatment does not alter desmocollin levels in *PKP2*$^{c.2013delC/WT}$ EHM. a, Representative immunoblots for DSC2 on PKP2 mutant and isogenic control EHM upon transduction with either AAV-ctr or AAV-PKP2. **b**, Quantification of (a). Colored dots represent distinct batches of differentiation, n = 4 technical replicates and 3 biological replicates. Data is presented as means +/− s.e.m. Statistical significance is derived by biological replicates and determined by one-way ANOVA (Tukey's post-hoc test) with p-value at $^{****}P < 0.0001$, $^{***}P < 0.001$, $^{**}P < 0.01$, $^{*}P < 0.05$, and not significant (ns). *P*-value = 0.0821.

https://doi.org/10.1038/s44161-023-00378-9

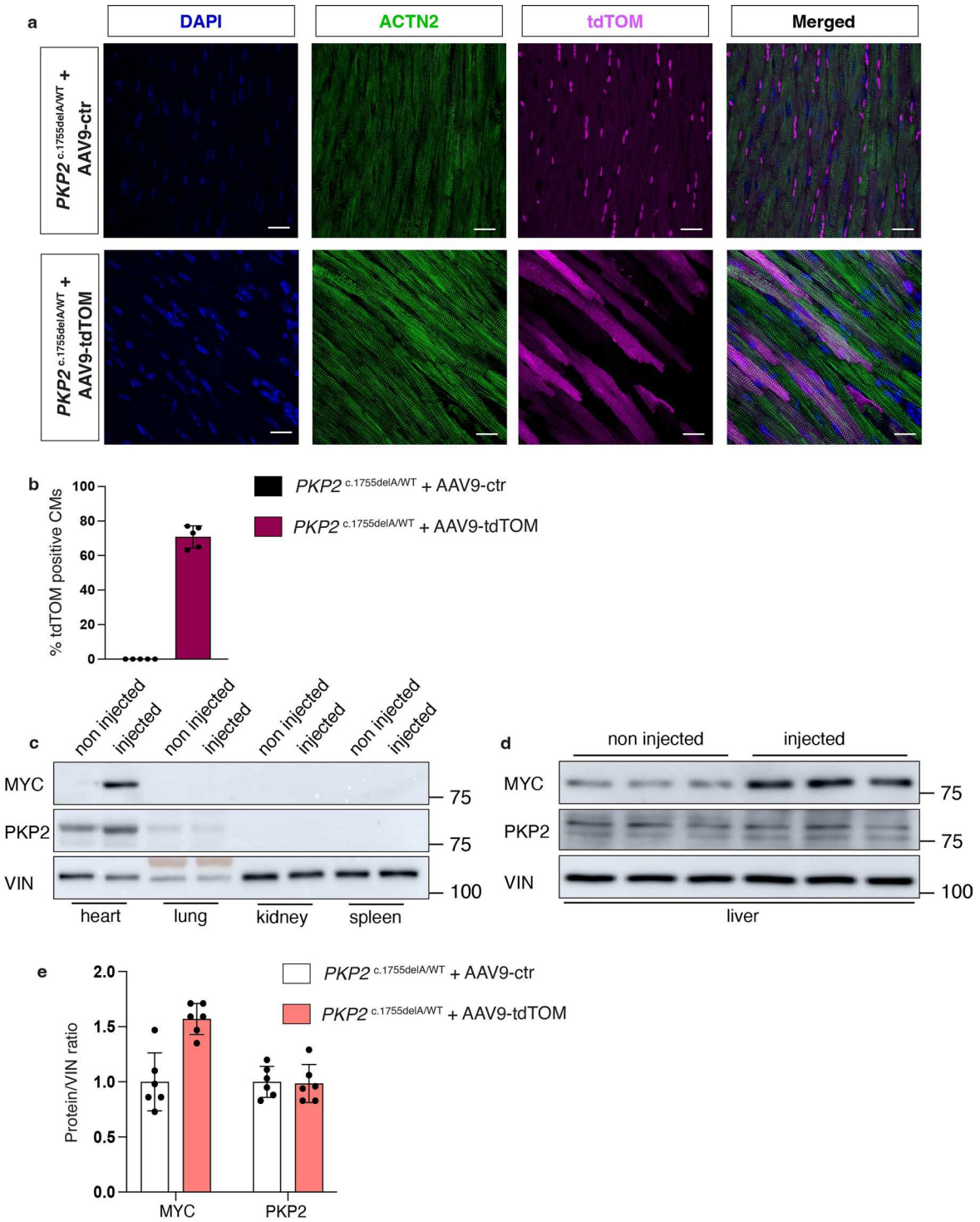

Extended Data Fig. 6 | AAV9 transduces cardiomyocytes *in vivo* with high efficiency and with minor ectopic expression. a, Immunofluorescence on cardiac sections of mice transduced with AAV9-tdTOM to facilitate transduction efficiency assessment. Nuclei = DAPI, ACTN2 = green, tdTOM = magenta. Scale bar is at 20µm. **b**, Quantification of (a), n = 5 hearts, 10 regions per heart were assessed. **c-d**, Immunoblot for MYC and PKP2 on protein lysates of different mouse tissues. VIN was used as a loading control. **e**, Quantification of (d), n = 5 mice per condition. Data is presented as means +/− s.e.m.

https://doi.org/10.1038/s44161-023-00378-9

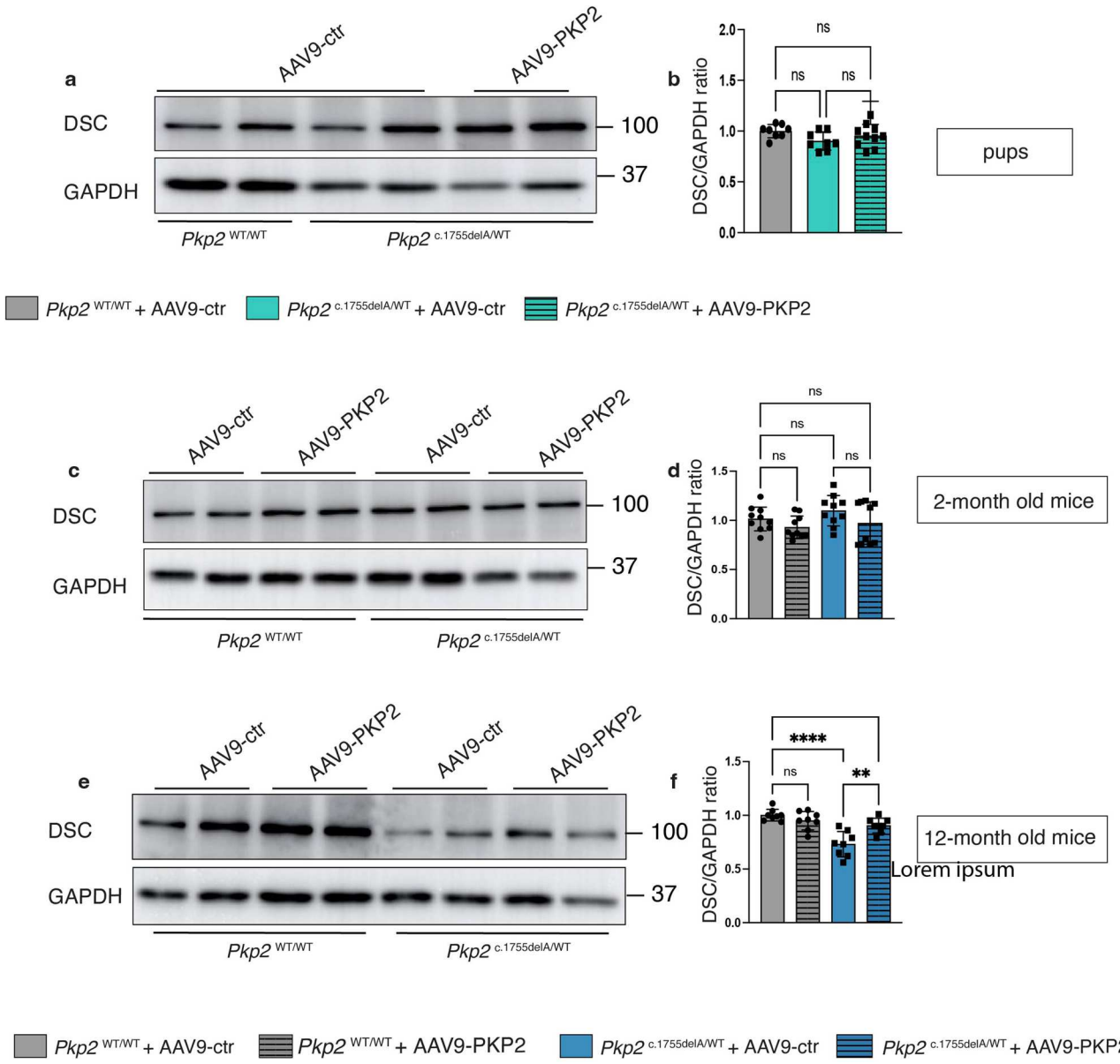

Extended Data Fig. 7 | DSC2 is not consistently responsive to PKP2 restoration in the Pkp2$^{c.1755delA/WT}$ murine models. a, c, e, Representative immunoblots for DSC2 in pups (n = 8,8 and 10 mice per group), 2-month-old (n = 10 mice per group) and 12-month-old mice (n = 8 mice per group) treated with AAV9-ctr or AAV9-PKP2. **b, d, f**, Quantification of each of the blots respectively. GAPDH has been used as a loading control for the quantification of the blots. Data is presented as mean +/− s.e.m. Statistical significance is determined by one-way ANOVA (Tukey's post-hoc test) with p-value at $^{****}P < 0.0001$, $^{***}P < 0.001$, $^{**}P < 0.01$, $^{*}P < 0.05$, and not significant (ns). *P*-value (f) = 0.0017.

https://doi.org/10.1038/s44161-023-00378-9

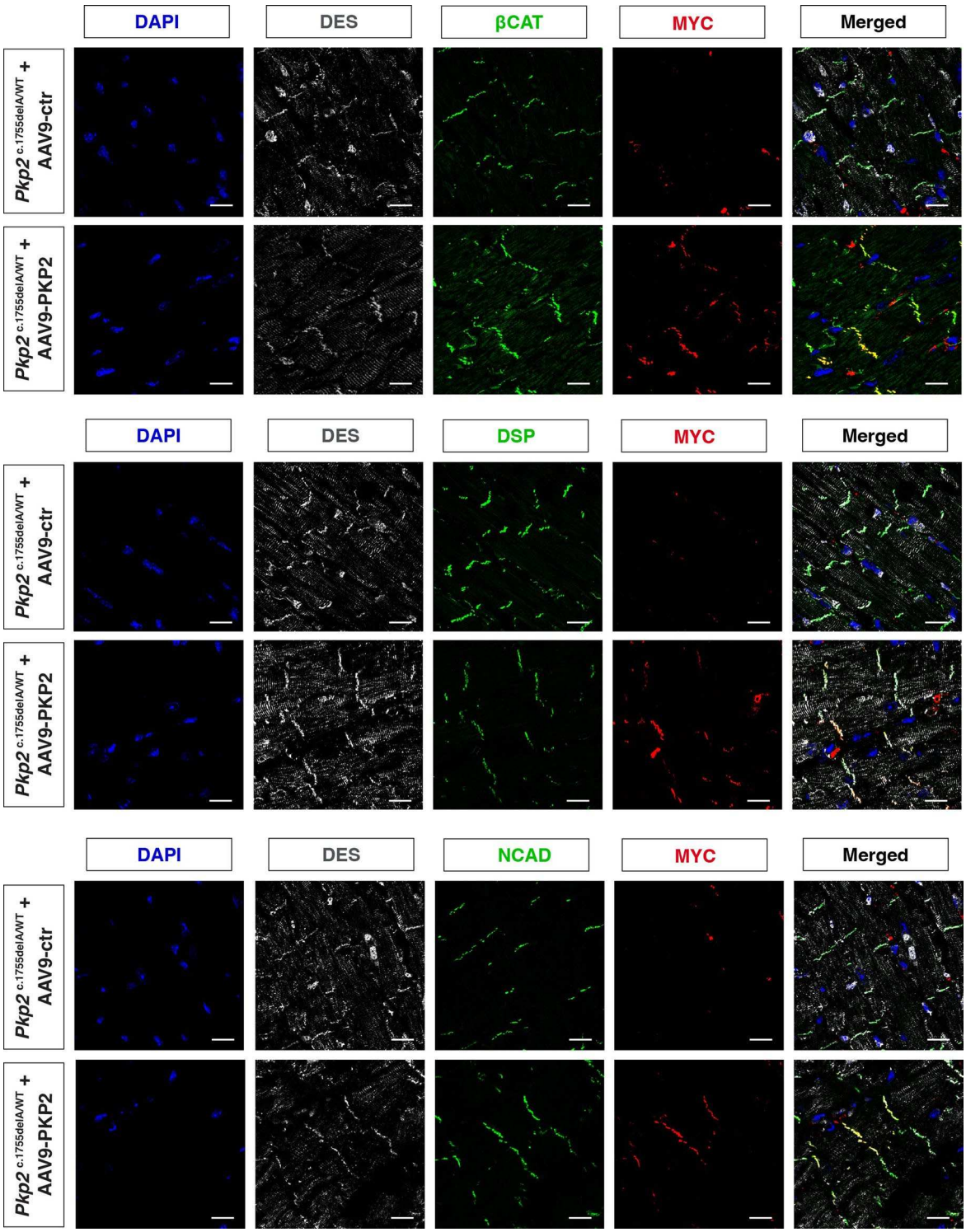

Extended Data Fig. 8 | The exogenously delivered PKP2 specifically localizes at the ID of cardiomyocytes together with more junctional proteins. Representative immunofluorescent images of the exogenous-specific marker MYC colocalizing βCAT (top row), DSP (middle row) and NCAD (bottom row). Scale bar is at 20μm. This experiment has been repeated independently 10 times (in 10 distinct mouse hearts) with similar results.

https://doi.org/10.1038/s44161-023-00378-9

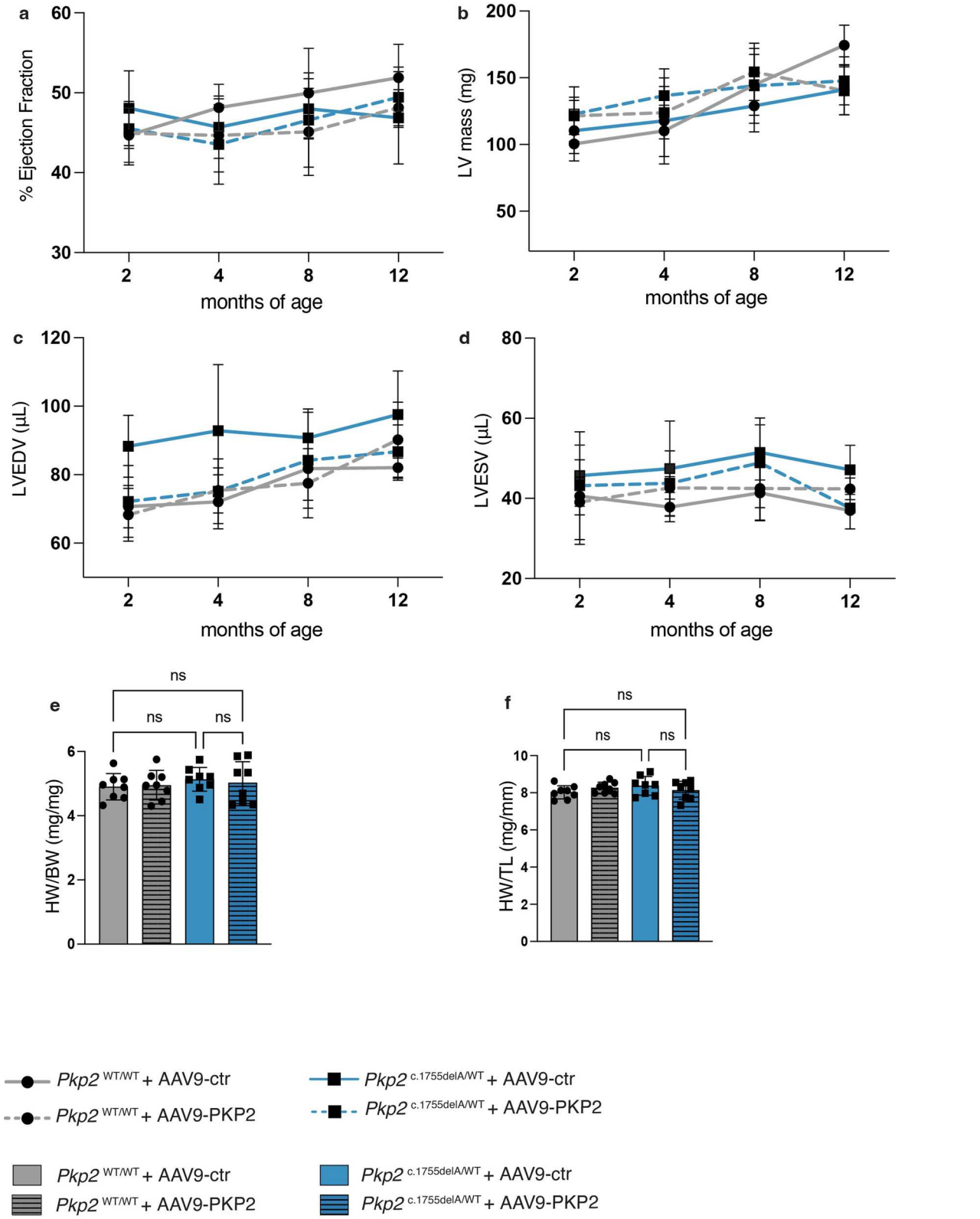

Extended Data Fig. 9 | AAV-mediated overexpression of *Pkp2* does not cause an overt adverse cardiac phenotype in *Pkp2*$^{WT/WT}$ 12-month-old mice. **a-d**, Trendlines showing % ejection fraction, left ventricle mass (LV mass), left ventricle end diastolic volume (LVEDV), left ventricle end systolic volume (LVESV) and in *Pkp2*$^{WT/WT}$ and *Pkp2*$^{c.1755delA/WT}$ mice treated with either AAV9-PKP2 or AAV9-ctr at baseline (2 months old), 2 months (4 months old), 6 months (8 months old) and 10 months (12 months old) post injection, n = 8 mice per condition. **e**, Heart weight (HW) to body weight (BW) ratio in *Pkp2*$^{WT/WT}$ and *Pkp2*$^{c.1755delA/WT}$ mice treated with either AAV9-PKP2 or AAV9-ctr, n = 8 mice per group. **f**, Heart weight to tibia length (TL) ratio in *Pkp2*$^{WT/WT}$ and *Pkp2*$^{c.1755delA/WT}$ mice treated with either AAV9-PKP2 or AAV9-ctr, n = 8 mice per group. Data is presented as means +/− s.e.m. Statistical significance is determined by one-way ANOVA (Tukey's post-hoc test), p-value at ****p < 0.0001, ***p < 0.001, **p < 0.01, *p < 0.05, and not significant (ns).

nature portfolio

Corresponding author(s): E van Rooij

Last updated by author(s): Oct 27, 2023

Reporting Summary

Nature Portfolio wishes to improve the reproducibility of the work that we publish. This form provides structure for consistency and transparency in reporting. For further information on Nature Portfolio policies, see our Editorial Policies and the Editorial Policy Checklist.

Statistics

For all statistical analyses, confirm that the following items are present in the figure legend, table legend, main text, or Methods section.

n/a	Confirmed	
☐	☒	The exact sample size (*n*) for each experimental group/condition, given as a discrete number and unit of measurement
☐	☒	A statement on whether measurements were taken from distinct samples or whether the same sample was measured repeatedly
☐	☒	The statistical test(s) used AND whether they are one- or two-sided *Only common tests should be described solely by name; describe more complex techniques in the Methods section.*
☒	☐	A description of all covariates tested
☐	☒	A description of any assumptions or corrections, such as tests of normality and adjustment for multiple comparisons
☒	☐	A full description of the statistical parameters including central tendency (e.g. means) or other basic estimates (e.g. regression coefficient) AND variation (e.g. standard deviation) or associated estimates of uncertainty (e.g. confidence intervals)
☐	☒	For null hypothesis testing, the test statistic (e.g. *F*, *t*, *r*) with confidence intervals, effect sizes, degrees of freedom and *P* value noted *Give P values as exact values whenever suitable.*
☒	☐	For Bayesian analysis, information on the choice of priors and Markov chain Monte Carlo settings
☒	☐	For hierarchical and complex designs, identification of the appropriate level for tests and full reporting of outcomes
☒	☐	Estimates of effect sizes (e.g. Cohen's *d*, Pearson's *r*), indicating how they were calculated

Our web collection on statistics for biologists contains articles on many of the points above.

Software and code

Policy information about availability of computer code

Data collection	Leica Application Suite (LAS X, version 3.30 or newer) was used for image acquisition of confocal microscopy data. Chemiluminescence on western blots was recorded using the ImageQuant software v7.1 of the Image Quant LAS 4000 Imaging System (GE Healthcare). Contractile function of EHM has been recorded by the custom-made MyrImager prototype software (MyriaMed GmbH)
Data analysis	Fiji (multiple versions between 2019 and 2023) was used for basic image analysis and adjustment of contrast and brightness. Chemiluminescence signal intensity was quantified using ImageQuant TL software v7.1 (GE Healthcare). Patch Control 384 software was used for the automated single cell patch clamp analysis (Nanion Technologies GmbH). The MyrImager prototype software was used for contraction analyses of the EHM. GraphPad Prism (version 9.5.1) was used for statistical analysis. Vevo Lab version 5.7.1 was used for echocardiography analysis.

For manuscripts utilizing custom algorithms or software that are central to the research but not yet described in published literature, software must be made available to editors and reviewers. We strongly encourage code deposition in a community repository (e.g. GitHub). See the Nature Portfolio guidelines for submitting code & software for further information.

Data

Policy information about availability of data

All manuscripts must include a data availability statement. This statement should provide the following information, where applicable:

- Accession codes, unique identifiers, or web links for publicly available datasets
- A description of any restrictions on data availability
- For clinical datasets or third party data, please ensure that the statement adheres to our policy

All data supporting the findings in this study are available within the paper and associated files. Source data are provided with this manuscript.

Research involving human participants, their data, or biological material

Policy information about studies with human participants or human data. See also policy information about sex, gender (identity/presentation), and sexual orientation and race, ethnicity and racism.

Reporting on sex and gender	n/a
Reporting on race, ethnicity, or other socially relevant groupings	n/a
Population characteristics	n/a
Recruitment	n/a
Ethics oversight	n/a

Note that full information on the approval of the study protocol must also be provided in the manuscript.

Field-specific reporting

Please select the one below that is the best fit for your research. If you are not sure, read the appropriate sections before making your selection.

☒ Life sciences ☐ Behavioural & social sciences ☐ Ecological, evolutionary & environmental sciences

For a reference copy of the document with all sections, see nature.com/documents/nr-reporting-summary-flat.pdf

Life sciences study design

All studies must disclose on these points even when the disclosure is negative.

Sample size	Sample size was predetermined for in vivo studies, using power analysis with type I error (alpha) = 0.05, type II error (beta) = 0.2 and effect size of 10%. For the in vitro studies, no specific sample size calculation was undertaken before experiments. We chose sample size according to previous experience in the field of molecular cardiology, which suggests that robust results have to be reproducible in at least three distinct biological replicates (cardiomyocyte differentiations).
Data exclusions	No data was excluded from the analysis.
Replication	All experiments were performed with a minimal of 3 replicates. Experiments in iPS-CM were performed in multiple (2 to 3) independent differentiations of the same iPS-cell line. The same applies for the studies using EHM tissues, where experiments were performed on tissues coming from 2-3 distinct differentiations. All independent experiments showed similar results, which confirmed reproducibility.
Randomization	Mice were allocated to groups based on their genotype. Where possible, littermate controls were used. Randomization was not relevant for in vitro experiments, however, all cells or samples were treated and analyzed in the same manner across conditions.
Blinding	Investigators were blinded to group allocation during data analysis (echo analysis, gene expression).

Reporting for specific materials, systems and methods

We require information from authors about some types of materials, experimental systems and methods used in many studies. Here, indicate whether each material, system or method listed is relevant to your study. If you are not sure if a list item applies to your research, read the appropriate section before selecting a response.

Materials & experimental systems

n/a	Involved in the study
☐	☒ Antibodies
☐	☒ Eukaryotic cell lines
☒	☐ Palaeontology and archaeology
☐	☒ Animals and other organisms
☒	☐ Clinical data
☒	☐ Dual use research of concern
☒	☐ Plants

Methods

n/a	Involved in the study
☒	☐ ChIP-seq
☒	☐ Flow cytometry
☒	☐ MRI-based neuroimaging

Antibodies

Antibodies used

A complete list with all details about the antibodies used in this study is provided in the supplemental tables 2 and 3. For all antibodies we have provided the supplier name, catalog number and working concentration.

Validation

Antibodies were used as directed by the suppliers. Below some statements from the supplier websites:

Plakophilin 2 (PKP2)-Abcam, ab189323- 1:100 (IF), 1:1000 (WB)-Supplier: Species reactivity include human, rat and mouse. Suitable for WB and IHP.

Anti-c-myc epitope tag [9B11]-Cell Signaling, #2276- 1:100 (IF), 1:1000 (WB)-Supplier: Myc-Tag (9B11) Mouse mAb detects exogenously expressed Myc-tagged proteins in cells expressed under a CMV promoter. Expression under other promoters has not been evaluated. Reactivity with all species.

ACTN2- Sigma Aldrich, HPA008315- 1:100 (IF)-Supplier: All Prestige Antibodies Powered by Atlas Antibodies are developed and validated by the Human Protein Atlas (HPA) project and as a result, are supported by the most extensive characterization in the industry. Species reactivity: human. Applications: Immunohistochemistry.

PKP2- BD Transduction laboratories, 610788- 1:1000 (WB)- Supplier: reactivity-QC testing:human, applications: western blot routinely tested

γ-catenin (D-12)- Santa Cruz, sc398183 - 1:1000 (WB) - Supplier: γ-catenin (D-12) is recommended for detection of γ-catenin of mouse, rat and human origin by Western Blotting (starting dilution 1:100, dilution range1:100-1:1000), immunoprecipitation [1-2 µg per 100-500 µg of total protein (1 ml of cell lysate)], immunofluorescence (starting dilution 1:50, dilutionrange 1:50-1:500) and solid phase ELISA (starting dilution 1:30, dilutionrange 1:30-1:3000).

Anti-desmoplakin I+II - Abcam, ab71690 - 1:1000 (WB) - Supplier: suitable for WB, ICC, IF. Reacts with human.

Desmocollin 2/3 Monoclonal Antibody (7G6) - Invitrogen, # 32-6200, 1:250 (WB), Supplier: This Antibody was verified by Relative expression to ensure that the antibody binds to the antigen stated. Species reactivity include human, mouse. Applications inlcude WB.

anti-Desmoglein 1/2 mouse monoclonal, DG 3.10, lyophilized, purified - Progen, 61002 - 1:100 (WB) - Supplier: Reactivity with bovine, human , rat. Tested applications include WB.

N-Cadherin (D4R1H) XP® Rabbit mAb - Cell Signaling, #13116, 1:1000 (WB) - Supplier: Applications include: WB, IP, IHC-Bond, IHC-P, IF-IC and species reactivity: mouse and human.

Anti-a-Catenin - Sigma Aldrich, C2081 - 1:1000 (WB) - Suppler: Anti-a-Catenin may be used for the immuno-localization of a-catenin by various immunohistochemical methods using frozen tissue sections and cultured cells. It may be used to detect a-catenin by other assays includingdot blot immunoassay and immunoblotting.

α-tubulin (α-tub) - Sigma Aldrich, T5168 - 1:1000 (WB) - Supplier: applications include western blot. Species reactivity include mouse and human.

Vinculin - Santa Cruz, sc-25336 - 1:1000 (WB) - Supplier: Species reactivity include human and mouse. Suitable for WB

β-catenin - Cell Signaling Technology, 8480S - 1:1000 (WB), 1:100 (IF), Species Reactivity: Human, Mouse, Rat (https://www.cellsignal.com/products/primary-antibodies/b-catenin-d10a8-xp-rabbit-mab/8480)

Desmin - https://www.rndsystems.com/products/human-mouse-desmin-antibody_af3844?gad_source=1&gclid=CjwKCAjwnOipBhBQEiwACyGLupYSlEhtHF_5Pe4QHMlPjarG2Ju8Lpeg0t1L_F_iSAHHmBmqFzq3BxoCQVQQAvD_BwE&gclsrc=aw.ds

Vimentin - https://datasheets.scbt.com/sc-373717.pdf

tdTomato - https://www.labome.com/product/SICGEN/AB8181-200.html

Horseradish peroxidase-coupled secondary antibodies - https://www.jacksonimmuno.com/catalog/products/315-035-003 and https://www.jacksonimmuno.com/catalog/products/211-035-109

Anti-Cardiac Troponin T antibody - https://www.abcam.com/en-is/products/primary-antibodies/anti-cardiac-troponin-t-antibody-ab45932

Alexa 488-anti-rabbit antibody - https://www.thermofisher.com/antibody/product/Donkey-anti-Rabbit-IgG-H-L-Highly-Cross-Adsorbed-Secondary-Antibody-Polyclonal/A-21206

Eukaryotic cell lines

Policy information about cell lines and Sex and Gender in Research

Cell line source(s)	The human PKP2 c.2013delC and PKP2 c.1849C>T iPSC lines were provided by H.-S. V. Chen at University of California San Diego45 and J. Wu at Stanford Cardiovascular Institute (supported by National Institutes of Health R24 HL117756), respectively.
Authentication	Authentication of the cells was not performed
Mycoplasma contamination	human iPSC were routinely monitored for mycoplasma contamination and tested negative.
Commonly misidentified lines (See ICLAC register)	No commonly misidentified lines were used.

Animals and other research organisms

Policy information about studies involving animals; ARRIVE guidelines recommended for reporting animal research, and Sex and Gender in Research

Laboratory animals	Mouse lines were maintained on C57B/6J background. PKP2 mutant mice as well. wildtype C57B/6J (Stock#: 000664) mice were obtained from Jackson Laboratories. Mice were housed under normal conditions with food and water ad libitum under normal day and night cycles in monitored environmental conditions. After the virus injection, the animals weree housed in DMI conditions for 2 weeks and until they reach the age of 1 year.
Wild animals	No wild animals were used in this study.
Reporting on sex	Animal studies involving pups included males and females. Animal studies involving adult animals (>8w) included males only.
Field-collected samples	No field-collected data are presented in this study.
Ethics oversight	Animal studies were approved by the animal welfare agency "Animal Welfare Body Utrecht" (IvD) of the Royal Dutch Academy of Sciences and Arts (KNAW) and in compliance with national legislation and institutional guidelines.

Note that full information on the approval of the study protocol must also be provided in the manuscript.